Title
Protein and Chemical Determinants of BL-1249 Action and Selectivity for K2P Channels

Journal
ACS Chemical Neuroscience, 9(12)

ISSN
1948-7193

Authors
Pope, Lianne
Arrigoni, Cristina
Lou, Hubing
et al.

Publication Date
2018-12-19

DOI
10.1021/acschemneuro.8b00337

Peer reviewed

ACS Chemical Neuroscience
Cite This: ACS Chem. Neurosci. 2018, 9, 3153−3165
Research Article
pubs.acs.org/chemneuro

Protein and Chemical Determinants of BL-1249 Action and Selectivity for K_{2P} Channels

Lianne Pope,[†] Cristina Arrigoni,[†] Hubing Lou,[†] Clifford Bryant,[‡] Alejandra Gallardo-Godoy,[‡] Adam R. Renslo,[‡] and Daniel L. Minor, Jr.*[,†,§,∥,⊥,#]

[†]Cardiovascular Research Institute, [‡]Department of Pharmaceutical Chemistry and Small Molecule Discovery Center, [§]Departments of Biochemistry and Biophysics, and Cellular and Molecular Pharmacology, [∥]California Institute for Quantitative Biomedical Research, and [⊥]Kavli Institute for Fundamental Neuroscience, University of California, San Francisco, California 93858-2330 United States

[#]Molecular Biophysics and Integrated Bio-imaging Division, Lawrence Berkeley National Laboratory, Berkeley, California 94720 United States

Supporting Information

ABSTRACT: K_{2P} potassium channels generate leak currents that stabilize the resting membrane potential of excitable cells. Various K_{2P} channels are implicated in pain, ischemia, depression, migraine, and anesthetic responses, making this family an attractive target for small molecule modulator development efforts. BL-1249, a compound from the fenamate class of nonsteroidal anti-inflammatory drugs is known to activate K_{2P}2.1 (TREK-1), the founding member of the thermo- and mechanosensitive TREK subfamily; however, its mechanism of action and effects on other K_{2P} channels are not well-defined. Here, we demonstrate that BL-1249 extracellular application activates all TREK subfamily members but has no effect on other K_{2P} subfamilies. Patch clamp experiments demonstrate that, similar to the diverse range of other chemical and physical TREK subfamily gating cues, BL-1249 stimulates the selectivity filter "C-type" gate that controls K_{2P} function. BL-1249 displays selectivity among the TREK subfamily, activating K_{2P}2.1(TREK-1) and K_{2P}10.1(TREK-2) ∼10-fold more potently than K_{2P}4.1(TRAAK). Investigation of mutants and K_{2P}2.1(TREK-1)/K_{2P}4.1(TRAAK) chimeras highlight the key roles of the C-terminal tail in BL-1249 action and identify the M2/M3 transmembrane helix interface as a key site of BL-1249 selectivity. Synthesis and characterization of a set of BL-1249 analogs demonstrates that both the tetrazole and opposing tetralin moieties are critical for function, whereas the conformational mobility between the two ring systems impacts selectivity. Together, our findings underscore the landscape of modes by which small molecules can affect K_{2P} channels and provide crucial information for the development of better and more selective K_{2P} modulators of the TREK subfamily.

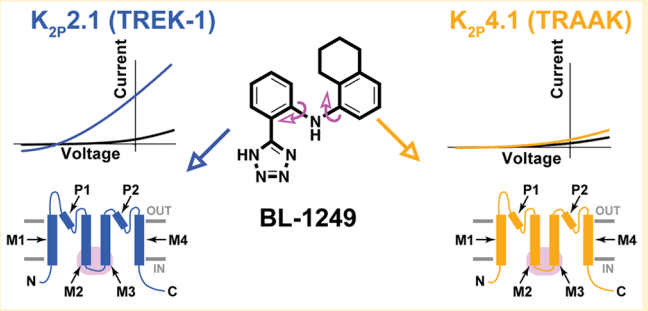

KEYWORDS: *K_{2P} channel, TREK channel, electrophysiology, ion channel chemical biology*

INTRODUCTION

K_{2P} (KCNK) potassium channels are members of the voltage-gated ion channel (VGIC) superfamily, make "background" or "leak" potassium channels that are responsible for the maintenance of cellular resting potential, and play an important role in regulating cellular excitability.[1−3] There are 15 K_{2P} subtypes that form six functionally distinct subfamilies. All K_{2P} channels comprise a dimer of subunits that each bear four transmembrane helices and two selectivity filter sequences.[1,4−7] In contrast to other VGIC superfamily members, the K_{2P} channel selectivity filter forms the principle gate that controls channel function, known as the "C-type gate", rather than an intracellular barrier formed by the pore-lining helices.[6,8−12] The activity of various K_{2P} subtypes has been linked to a variety of physiological and pathological processes including pain,[13−15] anesthetic responses,[16,17] arrhythmia,[18] ischemia,[16,19,20] depression,[21] and migraine.[22,23] Yet, despite these biological links, a paucity of K_{2P}-selective small molecule modulators has limited mechanistic and physiological studies.[1,24,25] Recent advances demonstrate that it is possible to develop subtype-selective K_{2P} small molecule modulators.[6,14,26−30] Such compounds and the knowledge of how they engage K_{2P} channels to modulate function open a path toward elaborating new K_{2P}-specific pharmacological tools that can enlighten channel gating mechanisms and that have potential to provide new leads for issues such as pain and ischemia.[25,31,32]

The TREK K_{2P} subfamily, comprising K_{2P}2.1(TREK-1), K_{2P}10.1(TREK-2), and K_{2P}4.1(TRAAK), is regulated by

Received: July 6, 2018
Accepted: August 8, 2018
Published: August 8, 2018

DOI: 10.1021/acschemneuro.8b00337
ACS Chem. Neurosci. 2018, 9, 3153−3165

diverse inputs that include temperature, stretch, pH, and lipids[1−3] and stands out as the most structurally elucidated K_{2P} subfamily.[4,6,7,33−35] TREK subfamily structures include examples of both inhibitor−channel[7] and activator−channel complexes[6] that highlight two points of control that can be influenced by small molecules: the transmembrane helices[7] and the K_{2P} modulator pocket.[6] Although these examples show how a small molecule can engage with the K_{2P} channel architecture to impact function, whether other reported TREK activators[14,26,28,36] act via the transmembrane domains or the K_{2P} modulator pocket or affect other K_{2P} channel elements remains to be elaborated.

Although not selective for K_{2P} channels, a number of fenamates, substituted derivatives of anthranilic acid,[37] activate members of the mechanosensitive TREK K_{2P} subfamily.[38,39] In particular, BL-1249, (5,6,7,8-tetrahydro-naphthalen-1-yl)-[2-(1*H*-tetrazol-5-yl)-phenyl]-amine, stimulates K_{2P}2.1(TREK-1)-like currents in bladder smooth muscle cells[39] and activates both K_{2P}2.1(TREK-1)[18,40] and K_{2P}10.1(TREK-2).[7] BL-1249 action is occluded by mutations that stabilize the C-type gate,[40] and activation by BL-1249 has been shown to reverse the functional effects of a K_{2P}2.1(TREK-1) genetic mutation implicated in right ventricular outflow tract (RVOT) tachycardia having a compromised ion selectivity.[18] Nevertheless, how BL-1249 stimulates K_{2P} activity and which elements of BL-1249 are crucial for its stimulatory effects have not yet been defined.

Here, we investigate the mechanism of action of BL-1249. Our studies show that this compound is a selective agonist of the TREK subfamily when applied extracellularly, having preferential action on K_{2P}2.1(TREK-1) and K_{2P}10.1(TREK-2) over K_{2P}4.1(TRAAK) and establish that its mechanism of action relies on gating at the selectivity filter C-type gate. Studies of a series of K_{2P}2.1(TREK-1)/K_{2P}4.1(TRAAK) chimeras and mutants indicate that the M2/M3 helices are key to BL-1249 action and identify residues in M2 that contribute to subtype selectivity. These findings indicate that BL-1249 acts at a separate site from the site of action of a structurally characterized activator, ML335, that directly stimulates the C-type gate via the K_{2P} modulator pocket.[6] Investigation of the functional properties of a set of BL-1249 analogs with respect to K_{2P} 2.1(TREK-1) and K_{2P} 4.1(TRAAK) show that both the acidic and tetralin moieties contribute to the stimulatory action of BL-1249 and indicate that the mobility of the two aryl rings relative to each other is key to the selective action of BL-1249 on K_{2P} 2.1(TREK-1).

RESULTS

BL-1249 External Application Differentially and Selectively Activates Mechanosensitive K_{2P} Channels. BL-1249 activates K_{2P}2.1(TREK-1)[18,40] and K_{2P}10.1(TREK-2),[7] but its effects on other K_{2P} channels have not been characterized. Hence, we sought to define how BL-1249 affected the two channels most closely related to K_{2P}2.1(TREK-1), K_{2P}10.1(TREK-2) and K_{2P}4.1(TRAAK), as well as representative members of the other K_{2P} subtypes: K_{2P}1.1(TWIK-1), K_{2P}3.1(TASK-1), K_{2P}5.1(TASK-2), K_{2P}9.1(TASK-3), K_{2P}13.1(THIK-1), and K_{2P}18.1(TRESK) (Figure 1A,B). Two-electrode voltage-clamp (TEVC) currents measured from *Xenopus* oocytes expressing each of the target channels showed clear activation responses after extracellular application of 10 μM BL-1249 for only K_{2P}2.1(TREK-1) and K_{2P}10.1(TREK-2). Measurement of the dose−response curves for these channels (Figure 1C) revealed similar EC_{50} values (5.5 ± 1.2 μM and 8.0 ± 0.8 μM for K_{2P}2.1(TREK-1) and K_{2P}10.1(TREK-2), respectively). Ten micromolar BL-1249 weakly stimulated K_{2P}4.1(TRAAK) in agreement with observations by Mathie and colleagues.[28] Measurement of the dose−response uncovered a robust response at higher concentrations that indicated a ∼10-fold reduction in the K_{2P}4.1(TRAAK) EC_{50} value relative to the other two TREK subfamily members (EC_{50}= 48 ± 10 μM, although complete saturation of the response could not be reached due to BL-1249 solubility limits, cf. Table 1; Figure 1C). In order to test if the original 10 μM assay had missed BL-1249 effects in other K_{2P} channels, we tested concentrations of BL-1249 up to the solubility limit (∼80 μM) against the other K_{2P} subfamily representatives. Despite the higher concentrations of BL-1249, we failed to find evidence for activation of the other K_{2P} subfamily representatives (Figure 1D). Thus, the data show that extracellular application of BL-1249 activates all members of the mechano- and thermosensitive TREK subfamily while sparing the other subfamilies and shows selectivity for K_{2P}2.1(TREK-1) and K_{2P}10.1(TREK-2) over K_{2P}4.1(TRAAK).

BL-1249 Activates the K_{2P}2.1(TREK-1) C-type Gate. Diverse types of physical and chemical stimuli activate K_{2P}2.1(TREK-1) by stabilizing the C-type gate and switching the channel into a "leak" mode that is characterized by a loss of outward rectification of the potassium current.[6,8] Accordingly, we used inside-out patch clamp experiments of K_{2P}2.1(TREK-1) expressed in HEK293 cells to test whether BL-1249 acts on the C-type gate. Application of 1 μM BL-1249 caused a clear loss of rectification similar to the effects reported for both physical and chemical activators of K_{2P}2.1(TREK-1) (Figure 2A−E).[6,8] Additionally, TEVC studies of the effects of BL-1249 on K_{2P}2.1(TREK-1) channels bearing mutations that activate the C-type gate, G137I and W275S,[6,10,41] demonstrated that these channels were insensitive to BL-1249 (Figure 2F). Together with previous single point concentration studies showing the insensitivity of K_{2P}2.1(TREK-1) W275S in mammalian cells,[40] our data provide definitive evidence that BL-1249 activates K_{2P}2.1(TREK-1) by stimulating the C-type gate. Thus, this compound fits the mechanistic paradigm shared by varied types of activators including mechanical stretch, pH, lipids, and small molecules.[6,8]

K_{2P} C-Terminal Tail Is Necessary for BL-1249 Action but Is Not the Sole Determinant of Channel Responsiveness. Gating stimuli detected by sensors in various parts of the channel converge on the K_{2P} selectivity filter C-type gate.[6,8,10,12,35] Because the C-terminal tail is the sensor for K_{2P}2.1(TREK-1) activation by both physiological[41−46] and chemical[45,47] activators, we asked whether uncoupling the C-terminal tail from the channel using a triple-glycine mutant at the M4/C-terminal tail junction, K_{2P}2.1(TREK-1)$_{GGG}$,[41] impacted the BL-1249 response. TEVC dose response studies of K_{2P}2.1(TREK-1)$_{GGG}$ showed that the effects of BL-1249 were significantly blunted relative to wild-type channels (EC_{50} = 19 ± 1 μM) (Figure 3A). This result contrasts previous studies of the small molecule activator ML67-33[26] for which uncoupling the C-terminal tail had no effect and suggests that unlike ML67-33, the C-terminal tail plays a role in mediating the BL-1249 response.

K_{2P}2.1(TREK-1) C-terminal truncations have been shown to reduce potentiation by other activating stimuli.[42,48] Hence, to probe the role of the C-terminal tail in the BL-1249 response further, we examined the effects of C-terminal tail truncations

DOI: 10.1021/acschemneuro.8b00337
ACS Chem. Neurosci. 2018, 9, 3153−3165

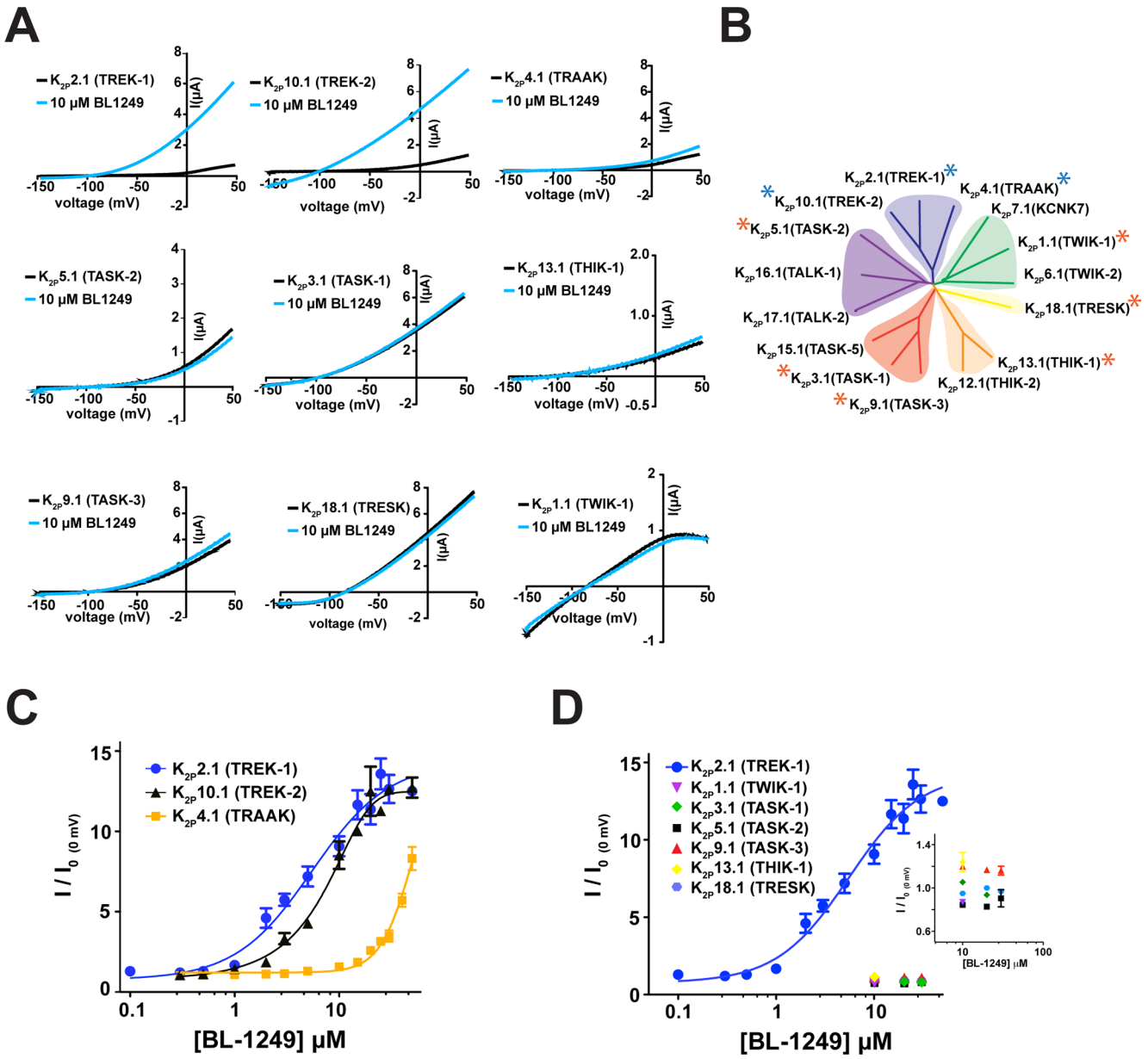

Figure 1. External application of BL-1249 selectively activates mechanosensitive K_{2P} channels. (A) Exemplar current traces for specified K_{2P} channels (black) with 10 μM BL-1249 (light blue) as measured via TEVC in *Xenopus* oocytes. (B) K_{2P} channel phylogenetic tree. Stars denote assayed representative K_{2P} channels. Blue stars indicate BL-1249 responsive channels. (C) BL-1249 dose−response curves for K_{2P}2.1(TREK-1) (blue circles), K_{2P}10.1(TREK-2) (black triangles), and K_{2P}4.1(TRAAK) (orange squares). EC_{50} = 5.5 ± 1.2 μM, 8.0 ± 0.8 μM, and 48 ± 10 μM, respectively. (D) BL-1249 responses of indicated K_{2P} channels. Inset shows expanded view of poorly responsive K_{2P} channels. Error bars are SEM.

at residue 322, K_{2P}2.1(TREK-1)$_{\Delta 322}$, equivalent to a previously described mutant called Δ89,[48] and at residue 308, K_{2P}2.1(TREK-1)$_{\Delta 308}$. Measurement of the dose−response curves for BL-1249 showed that these changes resulted in progressively reduced responses (EC_{50} = 26 ± 8 μM and 35 ± 8 μM for K_{2P}2.1(TREK-1)$_{\Delta 322}$ and K_{2P}2.1(TREK-1)$_{\Delta 308}$, respectively) (Figure 3B).

Given the importance of the C-terminal tail for the BL-1249 response and the fact that the C-terminal tails of K_{2P}2.1(TREK-1) and K_{2P}4.1(TRAAK) vary substantially (17.6% sequence similarity, 13.5% identity), we wondered if these differences could contribute to the different potencies observed in K_{2P}2.1(TREK-1) and K_{2P}4.1(TRAAK) BL-1249 responses. To test this possibility, we made chimeras that swapped the C-terminal tail between K_{2P}2.1(TREK-1) and K_{2P}4.1(TRAAK), TREK-1/AAK_T and TRAAK/EK_T. The TREK-1/AAK_T chimera yielded channels having responses similar to K_{2P}2.1(TREK-1) (EC_{50} = 7.7 ± 0.6 μM and 5.5 ± 1.2 μM for TREK-1/AAK_T and K_{2P}2.1(TREK-1), respectively; Figure 3C). By contrast, swapping the K_{2P}2.1(TREK-1) C-terminal tail onto K_{2P}4.1(TRAAK), TRAAK/EK-1_T, increased the sensitivity of K_{2P}4.1(TRAAK) core to BL-1249 by ~2-fold (EC_{50} = 23 ± 4 μM and 48 ± 10 μM, for TRAAK/EK-1_T and K_{2P}4.1(TRAAK) respectively) (Figure 3D). Despite this modest change, it is clear that the C-terminal tail alone is not sufficient to endow the K_{2P}4.1(TRAAK) core with a K_{2P}2.1(TREK-1)-like BL-1249 response. Although the C-terminal tail is not a major locus for the selective actions of BL-1249, the strong impact that uncoupling the C-terminal tail from the core channel and C-terminal tail truncations has on the K_{2P}2.1(TREK-1) response

DOI: 10.1021/acschemneuro.8b00337
ACS Chem. Neurosci. 2018, 9, 3153−3165

Table 1. Summary of K_{2P} Response to BL-1249[a]

background	mutant	EC_{50} (μM)	n ($\geq$)
K_{2P}2.1(TREK-1)		5.5 ± 1.2	3
	K_{2P}2.1(TREK-1)$_{GGG}$	19 ± 1	3
	K_{2P}2.1(TREK-1)$_{\Delta 322}$	26 ± 8[b]	2
	K_{2P}2.1(TREK-1)$_{\Delta 308}$	35 ± 8[b]	2
	TREK-1/AAK_T	7.7 ± 0.6	2
	TREK-1/AAK M4-C	19 ± 3	3
	TREK-1/AAK M3-C	28 ± 2	3
	TREK-1/AAK M2-C	39 ± 9	3
	TREK-1/TRAAK M2	26 ± 8	3
	F172M	15 ± 2	3
	F185L	27 ± 5	3
K_{2P}10.1(TREK-2)		8.0 ± 0.8	3
K_{2P}4.1(TRAAK)		48 ± 10[b]	3
	TRAAK/EK-1_T	23 ± 4	2
	TRAAK/EK-1 M4-C	45 ± 2	3
	TRAAK/EK-1 M3-C	18 ± 2	3
	TRAAK/EK-1 M2-C	28 ± 5	3
	TRAAK/TREK-1 M2	43 ± 11	3
	M134F	58 ± 34[b]	2
	L147F	27 ± 4	3

[a]Data derived from at least two independent experiments with each data point averaged from at least three oocytes. [b]Experiments where complete saturation of the response could not be reached due to BL-1249 solubility limits. For these cases, fits were imposed with an upper boundary of 15 (fold activation, I/I_0) to estimate EC_{50} and error.

to BL-1249 indicate that this channel element is an important factor that allows channel activation by BL-1249.

Multiple Transmembrane Regions Contribute to BL-1249 Activation. To look for other elements that might contribute to BL-1249 responses, we constructed a set of K_{2P}2.1(TREK-1)/K_{2P}4.1(TRAAK) chimeras in which an increasing amount of one channel was spliced with the other. For the purposes of nomenclature, the channels are named using the parent N-terminal portion and the C-terminal chimera junction even though the chimera set forms a continuum spanning the two wild-type channels (Figure 4A). For example, TREK-1/AAK M4-C bears the K_{2P}2.1(TREK-1) sequence up to the junction with M4, whereas TRAAK/EK-1 M2-C bears K_{2P}4.1(TRAAK) up to the junction with M2 even though the largest portion of both of these channels comes from K_{2P}2.1(TREK-1).

TEVC experiments showed that all of the chimeras formed functional channels (Figures S1 and S2). To test the ability of the chimeras to report on channel determinants for compound action, we examined the responses of the chimeras to two previously characterized activators, ML335, a compound that selectively activates K_{2P}2.1(TREK-1) but not K_{2P}4.1(TRAAK),[6] and ML67-33, an activator showing no clear preference for either channel.[26] The chimeras showed an essentially binary response to ML335 that was entirely dependent on the presence or absence of a lysine on the extracellular end of M4 that forms a cation−π interaction with ML335.[6] Only constructs bearing a lysine at position equivalent to K_{2P}2.1(TREK-1) residue 271 (K_{2P}2.1(TREK-1), TRAAK/EK-1 M2-C, TRAAK/EK-1 M3-C, and TREK-1/AAK M4-C) robustly responded to ML335 (Figure S1A−C,G). In contrast to these results, we found no major changes with respect to the responses of the various chimeras to ML67-33 (Figure S1D−F,H). These findings are consistent with the inability of ML67-33 to discriminate between K_{2P}2.1(TREK-1) and K_{2P}4.1(TRAAK).[26] Together, these studies show that this chimera set can identify selectivity determinants for activator compounds within the TREK subfamily.

We next examined how this panel of chimeras responded to BL-1249. We found that the character of the donor channel with respect to BL-1249 response became progressively prevalent as larger portions were swapped into the recipient channel, contrasting the binary changes seen for ML335 responses (Figures 4A−C and S1G, Table 1). Further, the patterns of changes in the BL-1249 responses were not equivalent with respect to the direction of the substitution. Substituting K_{2P}4.1(TRAAK) sequence into K_{2P}2.1(TREK-1) from the C-terminal direction caused stepwise changes in EC_{50} as the construct became dominated by the K_{2P}4.1(TRAAK) sequence (Figure 4A,C, clockwise in Figure 4A from K_{2P}2.1(TREK-1), EC_{50} = 5.5 ± 1.2, 19 ± 3, 28 ± 2, and 39 ± 9 μM for K_{2P}2.1(TREK-1), TREK-1/AAK M4-C, TREK-1/AAK M3-C, and TREK-1/AAK M2-C, respectively). By contrast, substitution of K_{2P}4.1(TRAAK) sequence into K_{2P}2.1(TREK-1) from the N-terminal direction caused a loss, mild recovery, and then further loss of BL-1249 response (Figure 4A,B, counterclockwise in Figure 4A from K_{2P}2.1(TREK-1), EC_{50} = 5.5 ± 1.2, 28 ± 5, 18 ± 2, 45 ± 2, and 48 ± 10 μM, for K_{2P}2.1(TREK-1), TRAAK/EK-1 M2-C, TRAAK/EK-1 M3-C, TRAAK/EK-1 M4-C, and K_{2P}4.1(TRAAK)). The complexity of the EC_{50} changes displayed by the chimeras with respect to BL-1249 contrasted with how these chimeras responded for the case in which there is a single site responsible for compound selectivity (Figure S1G). Such a contrast suggests that multiple parts of the channel make contributions that influence BL-1249 selectivity rather than just a single site.

K_{2P}2.1(TREK-1) M2 Residues Contribute to BL-1249 Selectivity. In the course of converting K_{2P}2.1(TREK-1) to K_{2P}4.1(TRAAK) and vice versa by chimeras, the M2/M3 region stood out as a point where we found both gradual changes in EC_{50} (i.e., TREK-1/AAK M3-C → TREK-1/AAK M2-C) and stepwise changes that reversed the general EC_{50} trend (i.e., TRAAK/EK-1 M3-C → TRAAK/EK-1 M2-C). To investigate this issue further, we generated two chimeras in which only the M2 helix was exchanged between K_{2P}2.1(TREK-1) and K_{2P}4.1(TRAAK), TREK-1/TRAAK M2 and TRAAK/TREK-1 M2. The substitution of the K_{2P}2.1(TREK-1) M2 helix into K_{2P}4.1(TRAAK) had little effect on the BL-1249 response, yielding a channel having a response indistinguishable from K_{2P}4.1(TRAAK) (EC_{50} = 43 ± 11 μM and 48 ± 10 μM for TRAAK/TREK-1 M2 and K_{2P}4.1(TRAAK), respectively) (Figure 5A). By contrast, the substitution of the K_{2P}4.1(TRAAK) M2 helix into K_{2P}2.1(TREK-1) caused a substantial loss in BL-1249 response (EC_{50} = 26 ± 8 μM and 5.5 ± 1.2 μM for TREK-1/TRAAK M2 and K_{2P}2.1(TREK-1), respectively), indicating that elements from M2 contribute to the K_{2P}2.1(TREK-1) response to BL-1249.

To identify K_{2P}2.1(TREK-1) M2 residues that might participate in the BL-1249 response, we mapped the residues that differ between K_{2P}2.1(TREK-1) and K_{2P}4.1(TRAAK) in the context of the K_{2P}2.1(TREK-1) structure[6] (Figure 5B,C). Two K_{2P}2.1(TREK-1) M2 residues stood out as candidates that could explain the reduction in BL-1249 response when the entire M2 helix was replaced with M2 from K_{2P}4.1(TRAAK). One is at the M2/M4 interface and occurs between Phe172 and Arg297 via a π−cation interaction that would be lost when Phe172 is replaced with the equivalent K_{2P}4.1(TRAAK)

DOI: 10.1021/acschemneuro.8b00337
ACS Chem. Neurosci. 2018, 9, 3153−3165

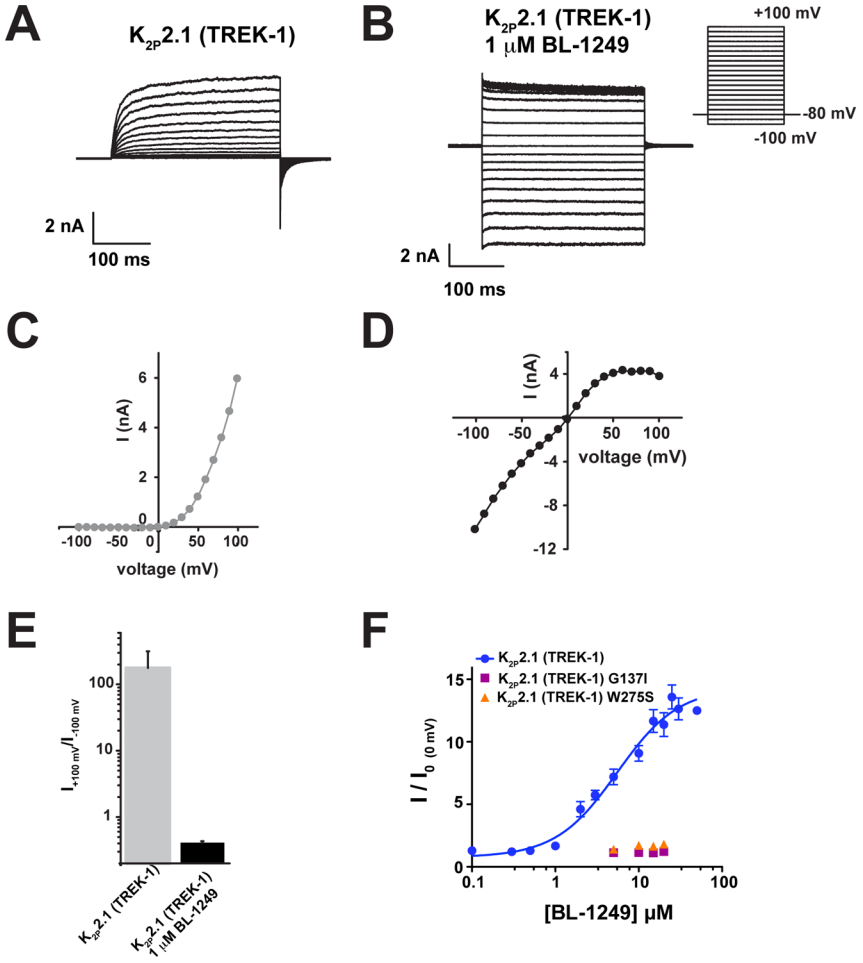

Figure 2. BL-1249 activates the K_{2P}2.1(TREK-1) C-type gate. (A, B) Exemplar current traces for (A) K_{2P}2.1(TREK-1) and (B) K_{2P}2.1(TREK-1) with 1 μM BL-1249 in HEK293 inside-out patches in 150 mM $K^+_{[out]}$/150 mM $Rb^+_{[in]}$. Inset shows voltage protocol. (C, D) Current−voltage relationships for (C) K_{2P}2.1(TREK-1) and (D) K_{2P}2.1(TREK-1) with 1 μM BL-1249. (E) Rectification coefficients (I_{+100mV}/I_{-100mV}) from recordings ($n \geq 3$) made in panels A−D. (F) Dose−response curves in *Xenopus* oocytes for K_{2P}2.1(TREK-1) (blue circles), K_{2P}2.1(TREK-1) G137I (purple squares), and K_{2P}2.1(TREK-1) W275S (orange triangles). K_{2P}2.1(TREK-1), 5.5 ± 1.2 μM; G137I and W275S, >60 μM. K_{2P}2.1(TREK-1) data are from Figure 1C. Error bars are SEM.

residue Met134 (Figure 5C, right inset). The second is an intrasubunit $\pi-\pi$ interaction between Phe185 from M2, a site whose equivalent in K_{2P}10.1(TREK-2) (Phe215) has a role in membrane stretch responses,[7] and Phe214 from M3 that would be disrupted by the replacement with the equivalent K_{2P}4.1(TRAAK) residue Leu147 (Figure 5C, left inset). To assess the importance of these interactions in the context of BL-1249 response, we made the K_{2P}2.1(TREK-1) mutants F172M and F185L and measured their responses to BL-1249 (Figure 5D). Both changes reduced the BL-1249 response (EC_{50} = 15 ± 2 μM and 27 ± 5 μM for F172M and F185L, respectively) to levels similar to the M2 helix swap. Notably, the M2/M3 interface substitution, F185L had a larger impact on the EC_{50}, whereas the M2/M4 change F172M caused a substantial reduction in the extent to which the channel could be activated by BL-1249 (Figure 5D). Unlike the case for K_{2P}2.1(TREK-1), the two corresponding inverse mutations in K_{2P}4.1(TRAAK), M134F at the M2/M4 interface and L147F at the M2/M3 interface did not cause similar outcomes. The mutation at the M2/M4 interface had no impact on BL-1249 response (EC_{50}, M134F 58 ± 34 μM), whereas the change in the M2/M3 interface conferred a modest improvement in the BL-1249 response (EC_{50}, L147F EC_{50} = 27 ± 4 μM; $p < 0.001$ at 35 μM (n = 7)) (Figure 5E). Taken together, these data highlight the importance of the M2 helix in BL-1249 activation. The observation that amino acid swaps in the M2/M3 interface are able to blunt the response of K_{2P}2.1(TREK-1) but enhance the response of K_{2P}4.1(TRAAK) points to the M2/M3 interface as a key element in the differential effects of BL-1249 on TREK subfamily members.

The BL-1249 Acidic Group and Tetralin Are Critical for Potency and Selectivity. Fenamates are weak K_{2P} modulators[38,39,49] and their structure−activity relationships (SAR) with respect to K_{2P} channels are poorly defined. Hence, we synthesized a set of BL-1249 derivatives in order to probe which portions of the small molecule were important for channel activation in the context of the differential responses of K_{2P}2.1(TREK-1) and K_{2P} 4.1(TRAAK). BL-1249 has two ring systems, one bearing a tetrazole and a second bearing a tetralin moiety. Replacement of the tetrazole by other similar functionalities resulted in compounds having poorer potency than BL-1249 against K_{2P}2.1(TREK-1) (EC_{50} = 22 ± 8 μM and 44 ± 10 μM for BL-1249-amide and BL-1249-acid, respectively; Figure 6A,B, Table 2). Notably, even though BL-1249-acid was slightly less potent than BL-1249-amide (~2-fold), it had a stronger stimulatory effect on the current than either BL-1249

DOI: 10.1021/acschemneuro.8b00337
ACS Chem. Neurosci. 2018, 9, 3153−3165

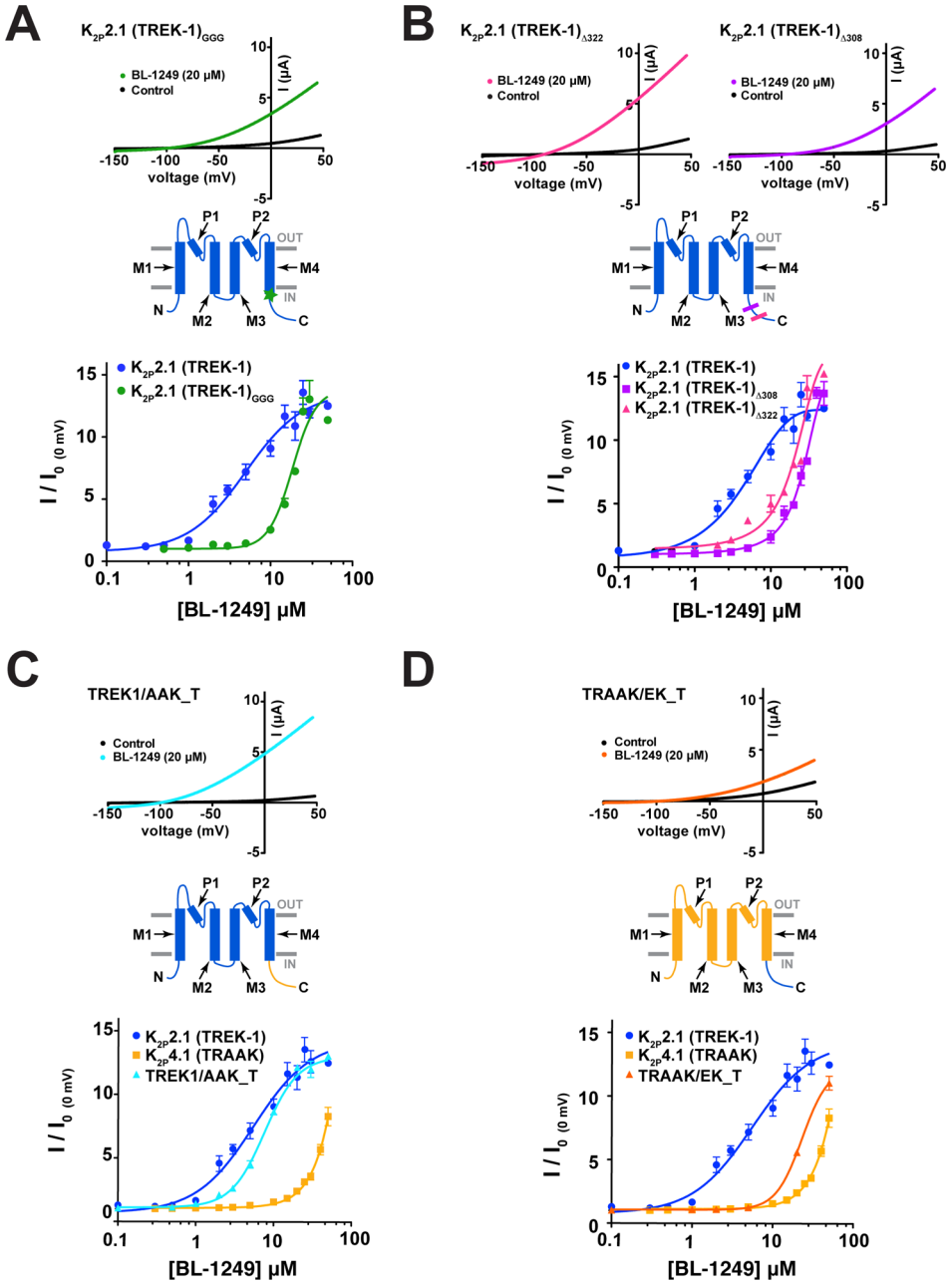

Figure 3. $K_{2P}2.1$(TREK-1) C-terminus affects BL-1249 response. (A) Exemplar current traces for $K_{2P}2.1$(TREK-1)$_{GGG}$ (black) with 20 μM BL-1249 (green) and BL-1249 dose−response curves for $K_{2P}2.1$(TREK-1) (blue circles) and $K_{2P}2.1$(TREK-1)$_{GGG}$ (green circles) (EC_{50} = 5.5 ± 1.2 μM and 19 ± 1 μM, respectively). Green star in cartoon indicates site of GGG mutation. (B) Exemplar current traces for $K_{2P}2.1$(TREK-1)$_{\mu 322}$ (magenta) and $K_{2P}2.1$(TREK-1)$_{\mu 308}$ (purple) with 20 μM BL-1249 and BL-1249 dose−response curves for $K_{2P}2.1$(TREK-1) (blue circles), $K_{2P}2.1$(TREK-1)$_{\Delta 322}$ (purple squares), and $K_{2P}2.1$(TREK-1)$_{\Delta 308}$ (magenta triangles). (EC_{50} = 5.5 ± 1.2 μM, 26 ± 8 μM, and 35 ± 8 μM, respectively). Magenta and purple lines in cartoon indicate sites of Δ322 and Δ308 truncations, respectively. (C) Exemplar current traces for TREK-1/AAK_T alone (black) and with 20 μM BL-1249 (cyan). BL-1249 dose−response curves for $K_{2P}2.1$(TREK-1) (blue circles), $K_{2P}4.1$(TRAAK) (light orange squares), and TRAAK/EK-1_T (light blue triangles). (EC_{50} = 5.5 ± 1.2 μM, 48 ± 10 μM, and 7.7 ± 0.6 μM, respectively). Cartoon indicates TREK-1/AAK_T channel regions from $K_{2P}2.1$ (blue) and $K_{2P}4.1$ (yellow). (D) Exemplar current traces for TRAAK/EK_T alone (black) and with 20 μM BL-1249 (orange). BL-1249 dose−response curves for $K_{2P}2.1$(TREK-1) (blue circles), $K_{2P}4.1$(TRAAK) (light orange squares), and TRAAK/EK_T (orange triangles) (EC_{50} = 5.5 ± 1.2 μM, 48 ± 10 μM, and 23 ± 4 μM, respectively). Cartoon indicates TRAAK/EK_T channel regions from $K_{2P}2.1$ (blue) and $K_{2P}4.1$ (light orange). In panels A−D, $K_{2P}2.1$(TREK-1) and $K_{2P}4.1$(TRAAK) data are from Figure 1C. Error bars are SEM.

or BL-1249-amide, suggesting that the acidic nature of the side chain is important for BL-1249 function (Figure 6B). Curiously, unlike what we observe for the TREK subfamily, for $K_{2P}18.1$(TRESK) the change from BL-1249 to BL-1249-acid has been reported to switch the functional effects of the compound from an activator to an inhibitor.[49] Both BL-1249-amide and BL-1249-acid retained selectively for $K_{2P}2.1$(TREK-1) over $K_{2P}4.1$(TRAAK) (Figure 6C,D) indicating that this moiety is not the key determinant of selectivity.

To test the importance of the tetralin moiety, we synthesized a BL-1249 derivative in which this entity was replaced by a simple phenyl ring (BL-1249-Ph) (Figure 6A). This substitution

DOI: 10.1021/acschemneuro.8b00337
ACS Chem. Neurosci. 2018, 9, 3153−3165

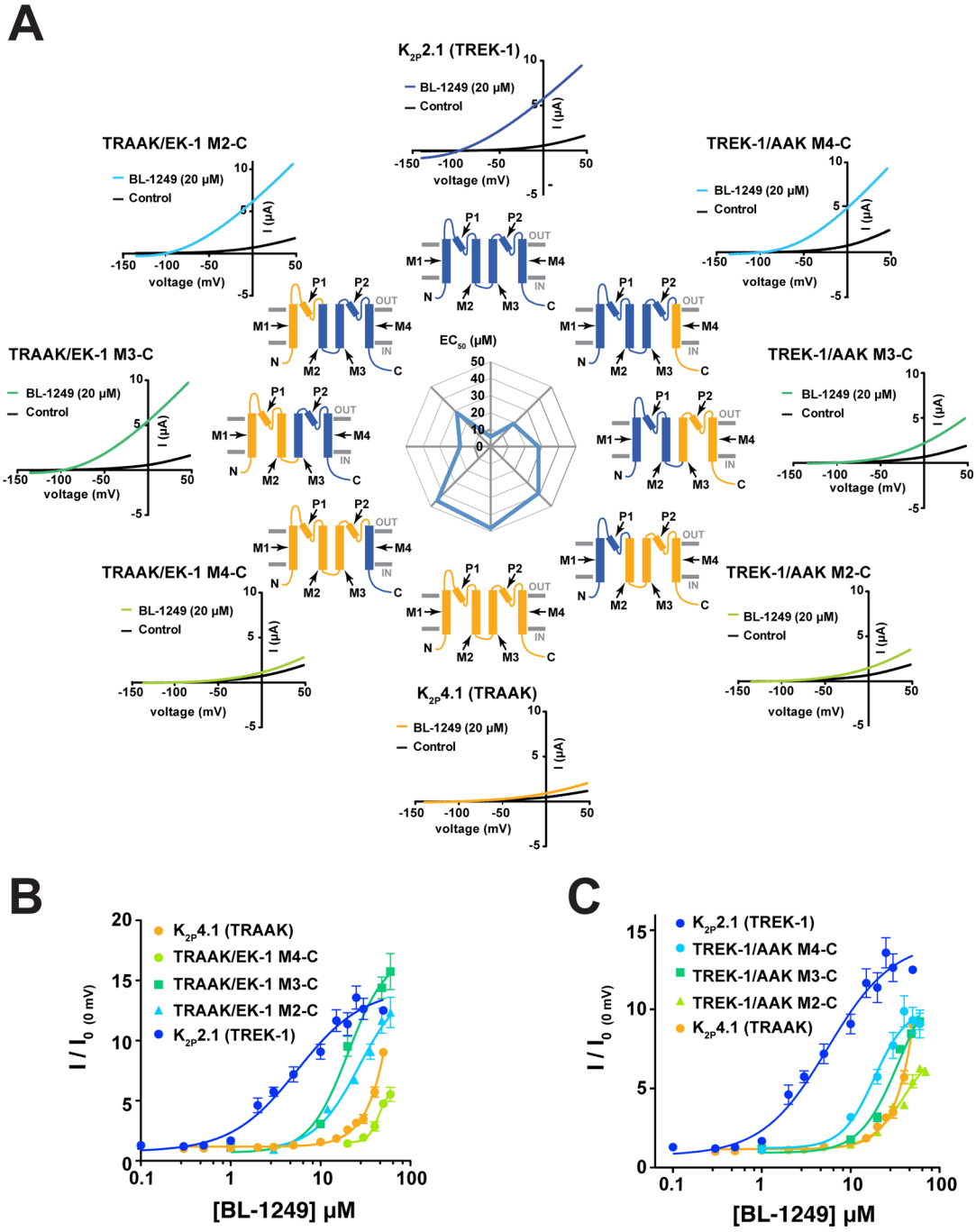

Figure 4. BL-1249 responses of TREK-1/TRAAK chimeras (A) Exemplar current traces for of BL-1249 responses for K_{2P}2.1(TREK-1) (blue), K_{2P}4.1(TRAAK) (light orange), and chimeras TREK-1/AAK M4-C (light blue), TREK-1/AAK M3-C (green), TREK-1/AAK M2-C (light green), TRAAK/EK-1 M4-C (light green), TRAAK/EK-1 M3-C (green), and TRAAK/EK-1 M2-C (light blue). Black and colored traces show basal and currents with 20 μM BL-1249, respectively. Cartoon schematics show channel portions from K_{2P}2.1(TREK-1) (blue) and K_{2P}4.1(TRAAK) (light orange). (B, C) Dose−response curves for K_{2P}2.1(TREK-1), K_{2P}4.1(TRAAK), and the indicated chimeras. (EC_{50} = 5.5 ± 1.2 μM, 48 ± 10 μM, 19 ± 3 μM, 28 ± 3 μM, 39 ± 9 μM, 45 ± 2 μM, 18 ± 2 μM, and 28 ± 5 μM for K_{2P}2.1(TREK-1), K_{2P}4.1(TRAAK), TREK-1/AAK M4-C, TREK-1/AAK M3-C, TREK-1/AAK M2-C, TRAAK/EK-1 M4-C, TRAAK/EK-1 M3-C, and TRAAK/EK-1 M2-C, respectively). K_{2P}2.1(TREK-1) and K_{2P}4.1(TRAAK) data are from Figure 1C. Error bars are SEM.

proved very detrimental to activity and yielded a compound that had only a small amount of stimulatory effect against K_{2P}2.1(TREK-1) (EC_{50} > 200 μM) and showed a similar profile against K_{2P}4.1(TRAAK) revealing the importance of the bicyclic tetralin ring for BL-1249 function (Figure 6B,E). Finally, we tested whether the conformation of the two aryl rings with respect to each other was important for the potency and selectivity of BL-1249. We made a BL-1249 derivative in which the tetralin structure was fused into a tricyclic scaffold to constrain the available conformations between the two aryl rings (BL-1249-tricycle) (Figure 6F). BL-1249-tricycle showed poorer activity against K_{2P}2.1(TREK-1) relative to BL-1249 (Figure 6G,H, EC_{50} = 34 ± 6 μM versus 5.5 ± 1.1 μM for BL-1249-tricycle and BL-1249, respectively) but, surprisingly, retained essentially the same activity against K_{2P}4.1(TRAAK) (Figure 6G,H, EC_{50} = 42 ± 9 μM versus 48 ± 10 μM for

DOI: 10.1021/acschemneuro.8b00337
ACS Chem. Neurosci. 2018, 9, 3153−3165

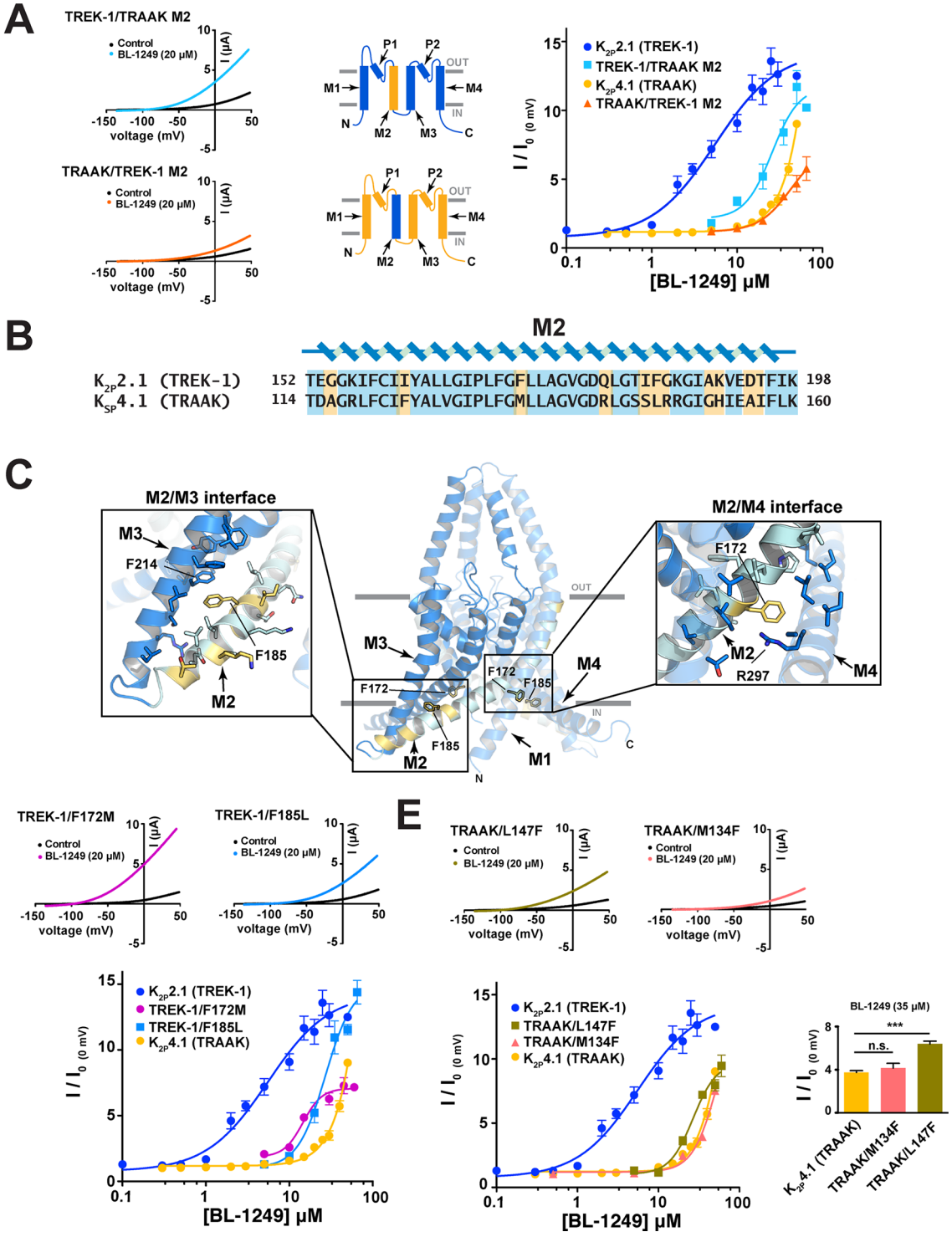

Figure 5. M2 residues contribute to BL-1249 selectivity between K_{2P}2.1(TREK-1) and K_{2P}4.1(TRAAK). (A) Exemplar current traces for TREK-1/TRAAK M2 (light blue) and TRAAK/TREK-1 M2 (orange) with 20 μM BL-1249 (left). Insets depict M2 helix swap. BL-1249 dose−response curves (right) for K_{2P}2.1(TREK-1) (blue circles), TREK-1/TRAAK M2 (light blue squares), K_{2P}4.1(TRAAK) (light orange circles), and TRAAK/TREK-1 M2 (orange triangles). (EC_{50} = 5.5 ± 1.2 μM, 26 ± 8 μM, 48 ± 10 μM, and 43 ± 11 μM, respectively). (B) Alignment of K_{2P}2.1(TREK-1) and K_{2P}4.1(TRAAK) M2 sequences. Nonconserved residues are highlighted in yellow. (C) K_{2P}2.1(TREK-1) (PDB 6CQ6)[6] structure. Residues that differ from K_{2P}4.1(TRAAK) are highlighted yellow. Panel insets show the environment surrounding the highlighted M2 residues. (D) Exemplar current traces for TREK-1/F172M (pink) and TREK-1/F185L (light blue), with 20 μM BL-1249. BL-1249 dose−response curves for K_{2P}2.1(TREK-1) (blue circles), TREK-1/F172M (pink circles), K_{2P}2.1 (F185L) (light blue squares), and K_{2P}4.1(TRAAK) (light orange circles). (EC_{50} = 5.5 ± 1.2 μM, 15 ± 2 μM, 27 ± 5 μM, and 48 ± 10 μM, respectively). (E) Exemplar current traces for TRAAK/M134F (orange triangles) and TRAAK/L147F (olive green squares) with 20 μM BL-1249. BL-1249 dose−response curves for K_{2P}2.1(TREK-1) (blue circles), TRAAK/M134F (orange triangles), TRAAK/L147F (olive green squares), and K_{2P}4.1(TRAAK) (light orange circles). (EC_{50} = 5.5 ± 1.2 μM, 58 ± 34 μM, 27 ± 4 μM, and 48 ± 10 μM, respectively). K_{2P}2.1(TREK-1) and K_{2P}4.1(TRAAK) data are from Figure 1C. Inset compares responses at 35 μM BL-1249: *** indicates $p < 0.001$ for a one-way ANOVA test; ns indicates no significant difference. Error bars are SEM.

DOI: 10.1021/acschemneuro.8b00337
ACS Chem. Neurosci. 2018, 9, 3153−3165

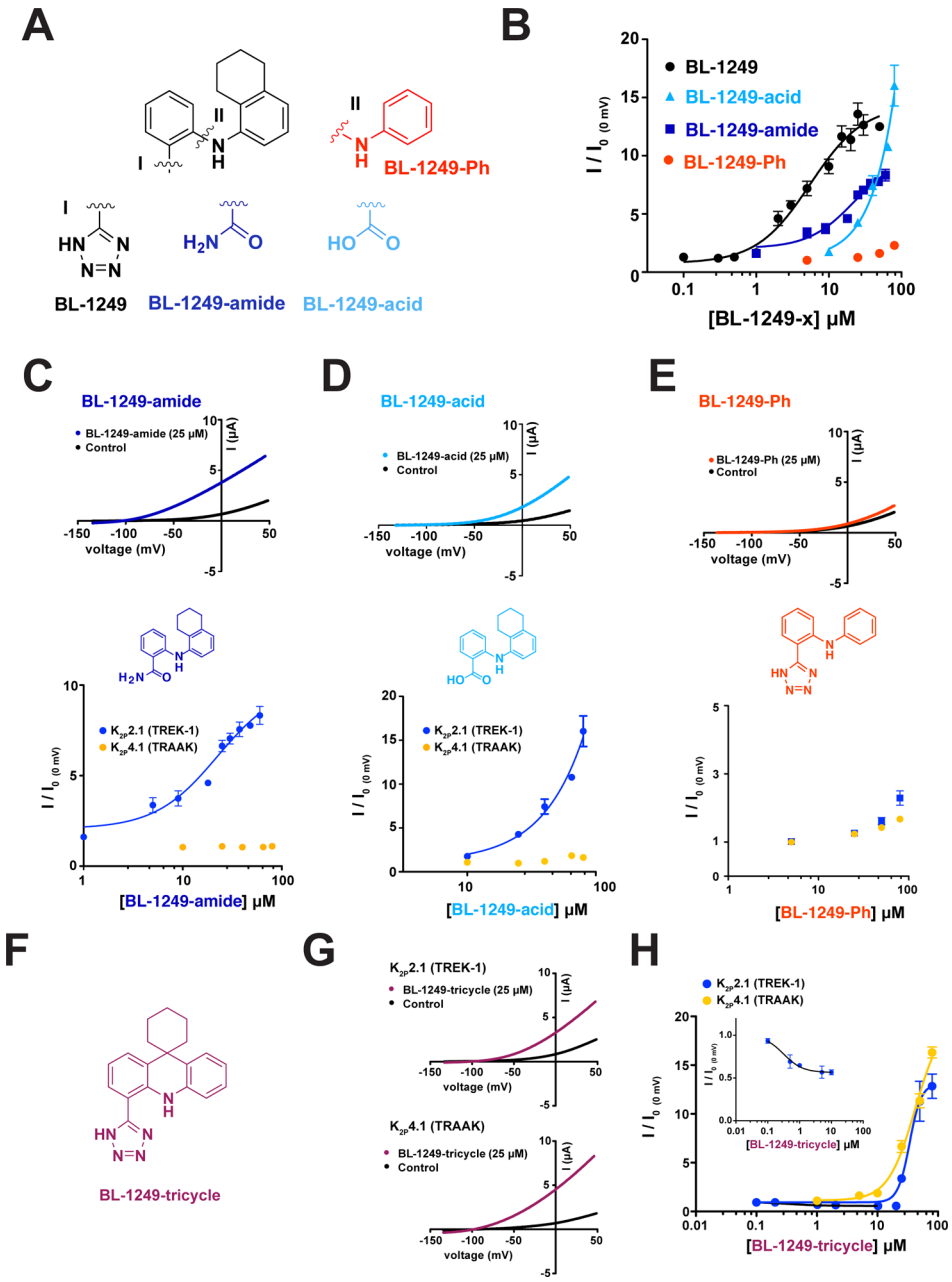

Figure 6. Structure−activity relationships of BL-1249 analogues. (A) Chemical structures of BL-1249 and analogues. "I" and "II" indicate the substitution sites. (B) Dose−response of K_{2P}2.1(TREK-1) for BL-1249 (black) (from Figure 1C), BL-1249-amide (blue), BL-1249-acid (light blue), and BL-1249-Ph (red) (EC_{50}= 5.5 ± 1.2 μM, 22 ± 8 μM, 44 ± 10 μM, and >100 μM, respectively). K_{2P}2.1(TREK-1) and K_{2P}4.1(TRAAK) data are from Figure 1C. (C−E) Exemplar current traces for K_{2P}2.1(TREK-1) with 25 μM BL-1249-amide (blue), BL-1249-acid (light blue), and BL-1249-Ph (red), respectively (top), chemical structures of BL-1249 analogues (middle), and dose response of K_{2P}2.1(TREK-1) (blue) and K_{2P}4.1(TRAAK) (light orange) (bottom). (F) Chemical structure of BL-1249-tricycle. (G) Exemplar current traces for K_{2P}2.1(TREK-1) and K_{2P}4.1(TRAAK) with 25 μM BL-1249-tricycle (purple). (H) Dose−response of K_{2P}2.1(TREK-1) (blue) and K_{2P}4.1(TRAAK) (light orange) for BL-1249-tricycle (EC_{50}= 34 ± 6 μM and 42 ± 9 μM, respectively). Error bars are SEM.

BL-1249-tricycle and BL-1249, respectively). This loss in selectivity between K_{2P}2.1(TREK-1) and K_{2P}4.1(TRAAK) indicates that the ability of the aryl and tetralin rings to adopt non-coplanar conformations is key to the preferential action of BL-1249 on K_{2P}2.1(TREK-1). We also observed that BL-1249-tricycle showed a small but robust "mode switch" behavior versus K_{2P}2.1(TREK-1) manifested as inhibition between 0.1 and 10 μM followed by activation at higher concentrations. This behavior was not evident against K_{2P}4.1(TRAAK) and further indicates the importance of the mobility between the two ring systems for the stimulatory action of BL-1249 on K_{2P}2.1(TREK-1). Notably, other tricyclic compounds have been reported to inhibit K_{2P}2.1(TREK-1) but not K_{2P}4.1(TRAAK)[50] similar to the properties of BL-1249-tricycle. Together, our studies demonstrate that both the acidic and tetralin moieties are important contributors to the stimulatory action of BL-1249 against K_{2P}2.1(TREK-1) and indicate that the mobility of the two aryl rings relative to each other is key to its selective effects on K_{2P}2.1(TREK-1) over K_{2P}4.1(TRAAK).

DOI: 10.1021/acschemneuro.8b00337
ACS Chem. Neurosci. 2018, 9, 3153−3165

Table 2. Summary of BL-1249 Analogue Activation of $K_{2P}2.1$(TREK-1) and $K_{2P}4.1$(TRAAK)[a]

compound	$K_{2P}2.1$(TREK-1) EC_{50} (μM)	n ($\geq$)	$K_{2P}4.1$(TRAAK) EC_{50} (μM)	n ($\geq$)
BL-1249	5.5 ± 1.2	3	48 ± 10[b]	3
BL-1249-amide	22 ± 8	3	>200	3
BL-1249-acid	44 ± 10[c]	4	>200	2
BL-1249-Ph	>200	3	>200	3
BL-1249-tricycle	34 ± 6	2	42 ± 9	3

[a]Data derived from at least two independent experiments with each data point averaged from at least three oocytes. [b]EC_{50} estimated imposing an upper boundary of 15 (fold activation, I/I_0). [c]EC_{50} estimated imposing an upper boundary of 20 (fold activation, I/I_0)

DISCUSSION

Addressing the relatively poor chemical biology surrounding the K_{2P} family is an important goal that has the potential to provide tool compounds that can remove the current barriers to understanding how diverse inputs modulate K_{2P} function, as well as the physiological roles of K_{2P} channels in various tissues.[1,24,25] Our studies show that the fenamic acid derivative BL-1249,[39] previously shown to activate $K_{2P}2.1$(TREK-1)[18,40] and $K_{2P}10.1$(TREK-2),[7] potently and selectively activates all three members of the mechanosensitive TREK K_{2P} subfamily, $K_{2P}2.1$(TREK-1), $K_{2P}10.1$(TREK-2), and $K_{2P}4.1$(TRAAK), by potentiating the potassium currents with EC_{50} values in the low micromolar range when applied extracellularly. Similar to many K_{2P} activators,[6,8,10,26,41] BL-1249 enhances TREK subfamily currents by stimulating the selectivity filter C-type gate. This mode of action provides further evidence for the central role of this C-type gate in the control of K_{2P} function.

There are currently two structurally characterized examples for how small molecules can engage members of the K_{2P} family. The cocrystal structure of $K_{2P}10.1$(TREK-2) with inhibitor norfluoxetine shows that this inhibitor binds in a pocket underneath the P2 helix of the selectivity filter at a site that is framed by the M2, M3, and M4 transmembrane helices and that becomes accessible when the pore lining M4 helix adopts a "down" conformation.[7,51] Although the binding site is clearly demarcated, how state-dependent binding of norfluoxetine inhibits is still unclear. Interestingly, besides inhibiting the movement of the M4 helix, the structural data indicates that the primary amine of norfluoxtine is near to the lower side of the selectivity filter where it could impact ion conduction by interfering with the electrostatic environment of the pore. The other structural example shows that a pair of related molecules, ML335 and ML402, bind to a cryptic binding site, the K_{2P} modulator pocket, situated behind the selectivity filter and sandwiched at the interface between the P1 pore helix and top of the M4 transmembrane helix of $K_{2P}2.1$(TREK-1).[6] These activators act as wedges that stabilize the mobility of the P1/M4 interface, a site also impacted by gain-of-function mutations,[6,10,35,41] and directly activate the C-type gate.[6] Understanding the extent to which other K_{2P} modulators, such as BL-1249 and ML67-33, act at the norfluoxetine site, the K_{2P} modulator pocket, or elsewhere on the channel is important for outlining the landscape of druggable sites for the K_{2P} potassium channel class.

Our studies of mutants and chimeras of $K_{2P}2.1$(TREK-1) and $K_{2P}4.1$(TRAAK) indicate that multiple channel elements that include C-terminal tail and the M2, M3, and M4 transmembrane helices contribute to BL-1249 responses. The integrity of the C-terminal tail is essential for BL-1249 stimulation (Figure 3), placing BL-1249 within a diverse class of TREK subfamily activators that are functionally dependent on this channel element including lipids,[42] arachidonic acid,[45] intracellular acidosis,[46] chloroform,[45] and temperature.[41] This dependence on the C-terminal tail is notably not shared by another tetrazole containing small molecule activator, ML67-33.[26] Despite the importance of the C-terminal tail in the BL-1249 response, our data indicate that this channel element has a limited role in mediating the selective action of BL-1249 on $K_{2P}2.1$(TREK-1) over $K_{2P}4.1$(TRAAK). By contrast, we do find evidence that multiple transmembrane domains contribute to BL-1249 selectivity. Although in the context of $K_{2P}2.1$(TREK-1)/$K_{2P}4.1$(TRAAK) chimeras no single transmembrane domain emerged as the predominant contributor, we were able to identify a site in the M2/M3 interface where exchange of a single amino acid between $K_{2P}2.1$(TREK-1) and $K_{2P}4.1$(TRAAK), F185L and L147F, respectively, was able to shift the BL-1249 phenotype in the direction of the donor channel, impairing the $K_{2P}2.1$(TREK-1) response while enhancing the $K_{2P}4.1$(TRAAK) response. Interestingly, the M2/M3 interface is also important for TREK subfamily responses to temperature[35] and membrane stretch.[52] Taken together, our findings suggest that BL-1249 does not act in the K_{2P} modulator pocket but affects a site that is a composite of elements from multiple transmembrane helices. Although this general characteristic is shared with the norfluoxetine site, the role of the M2/M3 interface in BL-1249 selectivity suggests that BL-1249 may act outside of both structurally defined small molecule sites.

Our studies of a small set of BL-1249 derivatives show that the two defining moieties of BL-1249, the tetrazole and the tetralin groups, contribute to the stimulatory effect of BL-1249 TREK subfamily channels. The acidic nature at the tetrazole site and the hydrophobicity of the tetralin ring are both crucial for the potency of BL-1249 (Figure 6). Whether or not the two rings are constrained is key for the compound to discriminate between $K_{2P}2.1$(TREK-1) and $K_{2P}4.1$(TRAAK) as demonstrated by the properties of BL-1249-tricycle. This dependence on the ability of the ring systems to adopt non-coplanar conformations in order to achieve selectivity within the TREK subfamily suggests that further exploration of strategies to modify the conformational preferences between the two ring systems might be a means to achieve better subtype discrimination. Interestingly, the importance of the tetrazole is a property shared by BL-1249 and ML67-33,[26] and both compounds share the general architecture of a hydrophobic ring system linked to the tetrazole. However, ML67-33 is not selective within the TREK subfamily and, rather than having hydrophobic moieties that can adopt a non-coplanar conformation, has an acridine ring system that is constrained, not unlike BL-1249-tricycle. This commonality between ML67-33 and BL-1249-tricycle lends further support to the idea that constrained versus conformationally adaptable hydrophobic ring systems are an important property for the tetrazole-bearing class of TREK subfamily activators. These shared features suggest that further optimization of hydrophobic scaffolds bearing tetrazoles or other acidic groups could provide a path toward the development of other TREK family modulators.

The actions of multiple diverse physical and chemical activators of the TREK subfamily converge at the C-type gate.[6,8−10,12,26,41] Our observation that BL-1249 also stimulates the C-type gate fits this paradigm. Our data support the idea that the BL-1249 site of action is not in the K_{2P} modulator pocket, the chemical

DOI: 10.1021/acschemneuro.8b00337
ACS Chem. Neurosci. 2018, 9, 3153−3165

modulator site closest to the C-type gate, but appears to reside among the transmembrane helices and supports the notion that changes in the channel architecture distant from the selectivity filter can impact the C-type gate.[6,35]

Elaboration of small molecule modulators for the TREK subfamily provides essential chemical biology tools for unraveling channel function and may offer new paths for treating issues such as pain[14,25] and arrhythmia.[18] Our study, together with recent structural work,[6,7] paints a complex landscape in which there are multiple points for small molecules to intervene in K_{2P} function. Given the growing and diverse list of small molecules that influence various K_{2P} channels,[14,26−28,36,50,53−57] further definition of the types of sites with which small molecules can bind and impact K_{2P} function through combined efforts of structural, functional, and computational studies will be crucial for defining how precise chemical control of K_{2P} activity can be achieved.

MATERIALS AND METHODS

Molecular Biology. Constructs for murine K_{2P} channels, including K_{2P}2.1(TREK-1) (Gene ID 16526), K_{2P}10.1(TREK-2) (Gene ID 72258), K_{2P}4.1(TRAAK) (Gene ID 16528), K_{2P}5.1(TASK-2) (Gene ID 16529), K_{2P}3.1(TASK-1) (Gene ID 16527), K_{2P}9.1(TASK-3) (Gene ID 223604), and K_{2P}18.1(TRESK) (Gene ID 332396) in pGEMHE/pMO, were used for *Xenopus* oocyte experiments as previously described.[10,26] Murine K_{2P}2.1(TREK-1) (Gene ID 16526) was expressed in HEK-293 cells using a pIRES-EGFP construct as previously described.[26] Murine K_{2P}13.1(THIK-1) (Gene ID 217826) and K_{2P}1.1(TWIK-1) (Gene ID 16525) were cloned into pGEMHE/pMO for use in *Xenopus* oocytes. Chimeras were designed using EMBOSS Needle pairwise sequence alignment tool[58] to match homologous helices in K_{2P}2.1(TREK-1) and K_{2P}4.1(TRAAK) and were assembled using the Gibson assembly method.[59] Chimera boundaries are Thr152 (TREK-1/AAK M2-C), Trp199 (TREK-1/AAK M3-C), Y272 (TREK-1/AAK M4-C), Thr114 (TRAAK/EK-1 M2-C), Trp161 (TRAAK/EK-1 M3-C), and Tyr234 K_{2P}4.1 (TRAAK). All sequences were verified using DNA sequencing.

Patch Clamp Electrophysiology. Mouse K_{2P}2.1 was expressed from a previously described pIRES2-EGFP vector in HEK293T cells (ATCC CRL-1573). Cells at 70% confluence were transfected (in 35 mm diameter wells) using LipofectAMINE 2000 (Invitrogen) for 6 h and plated onto coverslips coated with Matrigel (BD Biosciences).

Voltage-dependent activation of K_{2P}2.1 was recorded on excised patches in inside-out configuration (50 kHz sampling) in the absence and presence of 1 μM BL-1249. Pipette solution contained the following: 150 mM KCl, 3.6 mM $CaCl_2$, 10 mM HEPES (pH 7.4 with KOH). Bath solution contained the following: 150 mM RbCl, 2 mM EGTA, and 10 mM HEPES (pH 7.4 with RbOH), and it was continuously perfused at 200 mL/h during the experiment. TREK-1 currents were elicited by a 10 mV voltage step protocol from −100 mV to +100 mV, from a −80 mV holding potential. Data were analyzed using Clampfit 9 and Origin 7.

Two-Electrode Voltage-Clamp (TEVC) Electrophysiology. *Xenopus laevis* oocytes were harvested in accordance with UCSF IACUC protocol AN129690 and digested in calcium-free ND-96 (96 mM NaCl, 2 mM KCl, 3.8 mM $MgCl_2$) immediately following harvest, as previously described.[6,10] Digested oocytes were maintained in standard ND96 (96 mM NaCl, 2 mM KCl, 1.8 mM $CaCl_2$, 2 mM $MgCl_2$) with antibiotics (100 units mL^{-1} penicillin, 100 μg mL^{-1} streptomycin, 50 μg mL^{-1} gentimycin). Defolliculated stage V−VI oocytes were injected with 0.2−6.0 ng of mRNA in 50 nL, and currents were recorded 24−48 h after injection. mRNA was synthesized from plasmid DNA using mMessage mMachine Kit (T7 promoter, Ambion, Life Technologies) and purified using RNEasy Kit (Qiagen). Injected oocytes were impaled with two standard microelectrodes (0.2−1.0 MΩ) filled with 3 M KCl and subjected to constant perfusion of standard ND96 during recording. Currents were amplified using the GeneClamp 500B (MDS Analytical Technologies) amplifier controlled by the pClamp software (Molecular Devices). Data were digitized at 1 kHz using Digidata 1332A (MDS Analytical Technologies). For all experiments with small molecules, basal currents were evoked using 1 s long ramps from −150 to +50 mV under constant perfusion of ND96. Once stabilized basal currents were recorded, compounds were perfused at various concentrations in standard ND96 and currents were allowed to increase to stabilization before recording final current. Fold activation upon compound application is expressed as I/I_0 (0 mV), derived from the current at 0 mV in the presence of compound divided by the basal current at 0 mV in standard ND96 without compound. Data were analyzed and plotted using Graphpad Prism Version 5 (GraphPad Software, San Diego California USA, www.graphpad.com). In cases where saturation could not be reached due to BL-1249 solubility limits, EC_{50} was estimated using an upper bound of I/I_0 was set to 15 for the fits. In the case of BL-1249-acid EC_{50} estimation, upper bound of I/I_0 was set to 20 to account for the strong stimulation of BL-1249-acid.

BL-1249 Analogue Chemical Synthesis. Complete methods for the synthesis of BL-1249 analogs, BL-1249-acid, BL-1249-amide, BL-1249-Ph, and BL-1249-tricycle are found in the Supporting Information.

ASSOCIATED CONTENT

Supporting Information

The Supporting Information is available free of charge on the ACS Publications website at DOI: 10.1021/acschemneuro.8b00337.

Responses of TREK-1/TRAAK chimeras to ML355 and ML-67-33 and methods and schemes for synthesis of compounds (PDF)

AUTHOR INFORMATION

Corresponding Author

*E-mail: daniel.minor@ucsf.edu.

ORCID

Adam R. Renslo: 0000-0002-1240-2846

Daniel L. Minor, Jr.: 0000-0002-5998-4214

Author Contributions

L.P., C.A., H.L., and D.L.M. conceived the study and designed the experiments. L.P. and H.L. performed two-electrode voltage-clamp electrophysiology experiments. C.A. performed patch clamp electrophysiology experiments. L.P. and C.A. analyzed the electrophysiology data. L.P. and H.L. performed molecular biology experiments. C.B. and A.G.-G. synthesized and purified the compounds. C.B., A.G.-G., and A.R.R. designed the synthetic routes. D.L.M. analyzed data and provided guidance and support. L.P., C.A., C.B., A.R.R., and D.L.M. wrote the paper.

Notes

The authors declare no competing financial interest.

ACKNOWLEDGMENTS

We thank P. Riegelhaupt for input in the early stages of this project and K. Brejc for comments on the manuscript. This work was supported by Grant NIH-R01-MH093603 to D.L.M. and an American Heart Foundation Postdoctoral fellowship to C.A.

REFERENCES

(1) Feliciangeli, S., Chatelain, F. C., Bichet, D., and Lesage, F. (2015) The family of K channels: salient structural and functional properties. *J. Physiol. 593*, 2587.

(2) Enyedi, P., and Czirjak, G. (2010) Molecular background of leak K+ currents: two-pore domain potassium channels. *Physiol. Rev. 90*, 559−605.

(3) Renigunta, V., Schlichthorl, G., and Daut, J. (2015) Much more than a leak: structure and function of K(2)p-channels. *Pfluegers Arch. 467*, 867−894.

DOI: 10.1021/acschemneuro.8b00337
ACS Chem. Neurosci. 2018, 9, 3153−3165

(4) Brohawn, S. G., del Marmol, J., and MacKinnon, R. (2012) Crystal structure of the human K2P TRAAK, a lipid- and mechano-sensitive K+ ion channel. *Science 335*, 436−441.
(5) Miller, A. N., and Long, S. B. (2012) Crystal structure of the human two-pore domain potassium channel K2P1. *Science 335*, 432−436.
(6) Lolicato, M., Arrigoni, C., Mori, T., Sekioka, Y., Bryant, C., Clark, K. A., and Minor, D. L., Jr. (2017) K2P2.1 (TREK-1)-activator complexes reveal a cryptic selectivity filter binding site. *Nature 547*, 364−368.
(7) Dong, Y. Y., Pike, A. C., Mackenzie, A., McClenaghan, C., Aryal, P., Dong, L., Quigley, A., Grieben, M., Goubin, S., Mukhopadhyay, S., Ruda, G. F., Clausen, M. V., Cao, L., Brennan, P. E., Burgess-Brown, N. A., Sansom, M. S., Tucker, S. J., and Carpenter, E. P. (2015) K2P channel gating mechanisms revealed by structures of TREK-2 and a complex with Prozac. *Science 347*, 1256−1259.
(8) Schewe, M., Nematian-Ardestani, E., Sun, H., Musinszki, M., Cordeiro, S., Bucci, G., de Groot, B. L., Tucker, S. J., Rapedius, M., and Baukrowitz, T. (2016) A Non-canonical Voltage-Sensing Mechanism Controls Gating in K2P K(+) Channels. *Cell 164*, 937−949.
(9) Zilberberg, N., Ilan, N., and Goldstein, S. A. (2001) KCNKO: opening and closing the 2-P-domain potassium leak channel entails "C-type" gating of the outer pore. *Neuron 32*, 635−648.
(10) Bagriantsev, S. N., Peyronnet, R., Clark, K. A., Honore, E., and Minor, D. L., Jr. (2011) Multiple modalities converge on a common gate to control K2P channel function. *EMBO J. 30*, 3594−3606.
(11) Cohen, A., Ben-Abu, Y., Hen, S., and Zilberberg, N. (2008) A novel mechanism for human K2P2.1 channel gating. Facilitation of C-type gating by protonation of extracellular histidine residues. *J. Biol. Chem. 283*, 19448−19455.
(12) Piechotta, P. L., Rapedius, M., Stansfeld, P. J., Bollepalli, M. K., Erhlich, G., Andres-Enguix, I., Fritzenschaft, H., Decher, N., Sansom, M. S., Tucker, S. J., and Baukrowitz, T. (2011) The pore structure and gating mechanism of K2P channels. *EMBO J. 30*, 3607−3619.
(13) Devilliers, M., Busserolles, J., Lolignier, S., Deval, E., Pereira, V., Alloui, A., Christin, M., Mazet, B., Delmas, P., Noel, J., Lazdunski, M., and Eschalier, A. (2013) Activation of TREK-1 by morphine results in analgesia without adverse side effects. *Nat. Commun. 4*, 2941.
(14) Vivier, D., Soussia, I. B., Rodrigues, N., Lolignier, S., Devilliers, M., Chatelain, F. C., Prival, L., Chapuy, E., Bourdier, G., Bennis, K., Lesage, F., Eschalier, A., Busserolles, J., and Ducki, S. (2017) Development of the first Two-Pore Domain Potassium Channel TREK-1 (TWIK-Related K+ Channel 1)-selective agonist possessing in vivo anti-nociceptive activity. *J. Med. Chem. 60*, 1076.
(15) Alloui, A., Zimmermann, K., Mamet, J., Duprat, F., Noel, J., Chemin, J., Guy, N., Blondeau, N., Voilley, N., Rubat-Coudert, C., Borsotto, M., Romey, G., Heurteaux, C., Reeh, P., Eschalier, A., and Lazdunski, M. (2006) TREK-1, a K+ channel involved in polymodal pain perception. *EMBO J. 25*, 2368−2376.
(16) Heurteaux, C., Guy, N., Laigle, C., Blondeau, N., Duprat, F., Mazzuca, M., Lang-Lazdunski, L., Widmann, C., Zanzouri, M., Romey, G., and Lazdunski, M. (2004) TREK-1, a K+ channel involved in neuroprotection and general anesthesia. *EMBO J. 23*, 2684−2695.
(17) Lazarenko, R. M., Fortuna, M. G., Shi, Y., Mulkey, D. K., Takakura, A. C., Moreira, T. S., Guyenet, P. G., and Bayliss, D. A. (2010) Anesthetic activation of central respiratory chemoreceptor neurons involves inhibition of a THIK-1-like background K(+) current. *J. Neurosci. 30*, 9324−9334.
(18) Decher, N., Ortiz-Bonnin, B., Friedrich, C., Schewe, M., Kiper, A. K., Rinne, S., Seemann, G., Peyronnet, R., Zumhagen, S., Bustos, D., Kockskamper, J., Kohl, P., Just, S., Gonzalez, W., Baukrowitz, T., Stallmeyer, B., and Schulze-Bahr, E. (2017) Sodium permeable and "hypersensitive" TREK-1 channels cause ventricular tachycardia. *EMBO Mol. Med. 9*, 403−414.
(19) Laigle, C., Confort-Gouny, S., Le Fur, Y., Cozzone, P. J., and Viola, A. (2012) Deletion of TRAAK potassium channel affects brain metabolism and protects against ischemia. *PLoS One 7*, e53266.
(20) Wu, X., Liu, Y., Chen, X., Sun, Q., Tang, R., Wang, W., Yu, Z., and Xie, M. (2013) Involvement of TREK-1 activity in astrocyte function and neuroprotection under simulated ischemia conditions. *J. Mol. Neurosci. 49*, 499−506.
(21) Heurteaux, C., Lucas, G., Guy, N., El Yacoubi, M., Thummler, S., Peng, X. D., Noble, F., Blondeau, N., Widmann, C., Borsotto, M., Gobbi, G., Vaugeois, J. M., Debonnel, G., and Lazdunski, M. (2006) Deletion of the background potassium channel TREK-1 results in a depression-resistant phenotype. *Nat. Neurosci. 9*, 1134−1141.
(22) Andres-Enguix, I., Shang, L., Stansfeld, P. J., Morahan, J. M., Sansom, M. S., Lafreniere, R. G., Roy, B., Griffiths, L. R., Rouleau, G. A., Ebers, G. C., Cader, Z. M., and Tucker, S. J. (2012) Functional analysis of missense variants in the TRESK (KCNK18) K channel. *Sci. Rep. 2*, 237.
(23) Lafreniere, R. G., Cader, M. Z., Poulin, J. F., Andres-Enguix, I., Simoneau, M., Gupta, N., Boisvert, K., Lafreniere, F., McLaughlan, S., Dube, M. P., Marcinkiewicz, M. M., Ramagopalan, S., Ansorge, O., Brais, B., Sequeiros, J., Pereira-Monteiro, J. M., Griffiths, L. R., Tucker, S. J., Ebers, G., and Rouleau, G. A. (2010) A dominant-negative mutation in the TRESK potassium channel is linked to familial migraine with aura. *Nat. Med. 16*, 1157−1160.
(24) Mathie, A., and Veale, E. L. (2015) Two-pore domain potassium channels: potential therapeutic targets for the treatment of pain. *Pfluegers Arch. 467*, 931−943.
(25) Vivier, D., Bennis, K., Lesage, F., and Ducki, S. (2016) Perspectives on the Two-Pore Domain Potassium Channel TREK-1 (TWIK-Related K(+) Channel 1). A Novel Therapeutic Target? *J. Med. Chem. 59*, 5149−5157.
(26) Bagriantsev, S. N., Ang, K. H., Gallardo-Godoy, A., Clark, K. A., Arkin, M. R., Renslo, A. R., and Minor, D. L., Jr. (2013) A high-throughput functional screen identifies small molecule regulators of temperature- and mechano-sensitive K2P channels. *ACS Chem. Biol. 8*, 1841−1851.
(27) Su, Z. W., Brown, E. C., Wang, W. W., and MacKinnon, R. (2016) Novel cell-free high-throughput screening method for pharmacological tools targeting K+ channels. *Proc. Natl. Acad. Sci. U. S. A. 113*, 5748−5753.
(28) Loucif, A. J. C., Saintot, P. P., Liu, J., Antonio, B. M., Zellmer, S. G., Yoger, K., Veale, E. L., Wilbrey, A., Omoto, K., Cao, L., Gutteridge, A., Castle, N. A., Stevens, E. B., and Mathie, A. (2018) GI-530159, a novel, selective, mechanosensitive two-pore-domain potassium (K2P) channel opener, reduces rat dorsal root ganglion neuron excitability. *British journal of pharmacology 175*, 2272.
(29) Coburn, C. A., Luo, Y., Cui, M., Wang, J., Soll, R., Dong, J., Hu, B., Lyon, M. A., Santarelli, V. P., Kraus, R. L., Gregan, Y., Wang, Y., Fox, S. V., Binns, J., Doran, S. M., Reiss, D. R., Tannenbaum, P. L., Gotter, A. L., Meinke, P. T., and Renger, J. J. (2012) Discovery of a pharmacologically active antagonist of the two-pore-domain potassium channel K2P9.1 (TASK-3). *ChemMedChem 7*, 123−133.
(30) Rodrigues, N., Bennis, K., Vivier, D., Pereira, V., Chapuy, E., Deokar, H., Busserolles, J., Lesage, F., Eschalier, A., Ducki, S., and Chatelain, F. C. (2014) Synthesis and structure-activity relationship study of substituted caffeate esters as antinociceptive agents modulating the TREK-1 channel. *Eur. J. Med. Chem. 75*, 391−402.
(31) Bayliss, D. A., and Barrett, P. Q. (2008) Emerging roles for two-pore-domain potassium channels and their potential therapeutic impact. *Trends Pharmacol. Sci. 29*, 566−575.
(32) Yekkirala, A. S., Roberson, D. P., Bean, B. P., and Woolf, C. J. (2017) Breaking barriers to novel analgesic drug development. *Nat. Rev. Drug Discovery 16*, 545.
(33) Brohawn, S. G., Campbell, E. B., and MacKinnon, R. (2013) Domain-swapped chain connectivity and gated membrane access in a Fab-mediated crystal of the human TRAAK K+ channel. *Proc. Natl. Acad. Sci. U. S. A. 110*, 2129−2134.
(34) Brohawn, S. G., Campbell, E. B., and MacKinnon, R. (2014) Physical mechanism for gating and mechanosensitivity of the human TRAAK K+ channel. *Nature 516*, 126−130.
(35) Lolicato, M., Riegelhaupt, P. M., Arrigoni, C., Clark, K. A., and Minor, D. L., Jr. (2014) Transmembrane helix straightening and

DOI: 10.1021/acschemneuro.8b00337
ACS Chem. Neurosci. 2018, 9, 3153−3165

buckling underlies activation of mechanosensitive and thermosensitive K(2P) channels. *Neuron 84*, 1198−1212.
(36) Dadi, P. K., Vierra, N. C., Days, E. L., Dickerson, M., Vinson, P. N., Weaver, C. D., and Jacobson, D. A. (2017) Selective small molecule activators of TREK-2 channels stimulate DRG c-fiber nociceptor K2P currents and limit calcium influx. *ACS Chem. Neurosci. 8*, 558.
(37) Graham, G. G. (2016) Fenamates, in *Compendium of Inflammatory Diseases* (Parnham, M. J., Ed.), pp 477−482, Springer Basel, Basel.
(38) Takahira, M., Sakurai, M., Sakurada, N., and Sugiyama, K. (2005) Fenamates and diltiazem modulate lipid-sensitive mechano-gated 2P domain K(+) channels. *Pfluegers Arch. 451*, 474−478.
(39) Tertyshnikova, S., Knox, R. J., Plym, M. J., Thalody, G., Griffin, C., Neelands, T., Harden, D. G., Signor, L., Weaver, D., Myers, R. A., and Lodge, N. J. (2005) BL-1249 [(5,6,7,8-tetrahydro-naphthalen-1-yl)-[2-(1H-tetrazol-5-yl)-phenyl]-amine]: a putative potassium channel opener with bladder-relaxant properties. *J. Pharmacol. Exp. Ther. 313*, 250−259.
(40) Veale, E. L., Al-Moubarak, E., Bajaria, N., Omoto, K., Cao, L., Tucker, S. J., Stevens, E. B., and Mathie, A. (2014) Influence of the N terminus on the biophysical properties and pharmacology of TREK1 potassium channels. *Mol. Pharmacol. 85*, 671−681.
(41) Bagriantsev, S. N., Clark, K. A., and Minor, D. L., Jr. (2012) Metabolic and thermal stimuli control K(2P)2.1 (TREK-1) through modular sensory and gating domains. *EMBO J. 31*, 3297−3308.
(42) Chemin, J., Patel, A. J., Duprat, F., Lauritzen, I., Lazdunski, M., and Honore, E. (2005) A phospholipid sensor controls mechanogating of the K+ channel TREK-1. *EMBO J. 24*, 44−53.
(43) Chemin, J., Patel, A. J., Duprat, F., Sachs, F., Lazdunski, M., and Honore, E. (2007) Up- and down-regulation of the mechano-gated K(2P) channel TREK-1 by PIP (2) and other membrane phospholipids. *Pfluegers Arch. 455*, 97−103.
(44) Murbartian, J., Lei, Q., Sando, J. J., and Bayliss, D. A. (2005) Sequential phosphorylation mediates receptor- and kinase-induced inhibition of TREK-1 background potassium channels. *J. Biol. Chem. 280*, 30175−30184.
(45) Patel, A. J., Honore, E., Maingret, F., Lesage, F., Fink, M., Duprat, F., and Lazdunski, M. (1998) A mammalian two pore domain mechano-gated S-like K+ channel. *EMBO J. 17*, 4283−4290.
(46) Honore, E., Maingret, F., Lazdunski, M., and Patel, A. J. (2002) An intracellular proton sensor commands lipid- and mechano-gating of the K(+) channel TREK-1. *EMBO J. 21*, 2968−2976.
(47) Lotshaw, D. P. (2007) Biophysical, pharmacological, and functional characteristics of cloned and native mammalian two-pore domain K+ channels. *Cell Biochem. Biophys. 47*, 209−256.
(48) Maingret, F., Honore, E., Lazdunski, M., and Patel, A. J. (2002) Molecular basis of the voltage-dependent gating of TREK-1, a mechano-sensitive K(+) channel. *Biochem. Biophys. Res. Commun. 292*, 339−346.
(49) Monteillier, A., Loucif, A., Omoto, K., Stevens, E. B., Lainez, S., Saintot, P. P., Cao, L., and Pryde, D. C. (2016) Investigation of the structure activity relationship of flufenamic acid derivatives at the human TRESK channel K2P18.1. *Bioorg. Med. Chem. Lett. 26*, 4919−4924.
(50) Thummler, S., Duprat, F., and Lazdunski, M. (2007) Antipsychotics inhibit TREK but not TRAAK channels. *Biochem. Biophys. Res. Commun. 354*, 284−289.
(51) McClenaghan, C., Schewe, M., Aryal, P., Carpenter, E. P., Baukrowitz, T., and Tucker, S. J. (2016) Polymodal activation of the TREK-2 K2P channel produces structurally distinct open states. *J. Gen. Physiol. 147*, 497−505.
(52) Aryal, P., Jarerattanachat, V., Clausen, M. V., Schewe, M., McClenaghan, C., Argent, L., Conrad, L. J., Dong, Y. Y., Pike, A. C. W., Carpenter, E. P., Baukrowitz, T., Sansom, M. S. P., and Tucker, S. J. (2017) Bilayer-Mediated Structural Transitions Control Mechanosensitivity of the TREK-2 K2P Channel. *Structure 25*, 708−718e702.
(53) Braun, G., Lengyel, M., Enyedi, P., and Czirjak, G. (2015) Differential sensitivity of TREK-1, TREK-2 and TRAAK background potassium channels to the polycationic dye ruthenium red. *British journal of pharmacology 172*, 1728−1738.
(54) Chokshi, R. H., Larsen, A. T., Bhayana, B., and Cotten, J. F. (2015) Breathing Stimulant Compounds Inhibit TASK-3 Potassium Channel Function Likely by Binding at a Common Site in the Channel Pore. *Mol. Pharmacol. 88*, 926−934.
(55) Luethy, A., Boghosian, J. D., Srikantha, R., and Cotten, J. F. (2017) Halogenated Ether, Alcohol, and Alkane Anesthetics Activate TASK-3 Tandem Pore Potassium Channels Likely through a Common Mechanism. *Mol. Pharmacol. 91*, 620−629.
(56) Kennard, L. E., Chumbley, J. R., Ranatunga, K. M., Armstrong, S. J., Veale, E. L., and Mathie, A. (2005) Inhibition of the human two-pore domain potassium channel, TREK-1, by fluoxetine and its metabolite norfluoxetine. *Br. J. Pharmacol. 144*, 821−829.
(57) Patel, A. J., Honore, E., Lesage, F., Fink, M., Romey, G., and Lazdunski, M. (1999) Inhalational anesthetics activate two-pore-domain background K+ channels. *Nat. Neurosci. 2*, 422−426.
(58) Rice, P., Longden, I., and Bleasby, A. (2000) EMBOSS: the European Molecular Biology Open Software Suite. *Trends Genet. 16*, 276−277.
(59) Gibson, D. G., Young, L., Chuang, R. Y., Venter, J. C., Hutchison, C. A., 3rd, and Smith, H. O. (2009) Enzymatic assembly of DNA molecules up to several hundred kilobases. *Nat. Methods 6*, 343−345.

DOI: 10.1021/acschemneuro.8b00337
ACS Chem. Neurosci. 2018, 9, 3153−3165

Supporting Information for

Protein and chemical determinants of BL-1249 action and selectivity for K_{2P} channels

Lianne Pope[1], Cristina Arrigoni[1], Hubing Lou[1], Clifford Bryant[2], Alejandra Gallardo-Godoy[2], Adam R. Renslo[2], and Daniel L. Minor, Jr.[1-5*]

[1]Cardiovascular Research Institute

[2]Department of Pharmaceutical Chemistry and Small Molecule Discovery Center

[3]Departments of Biochemistry and Biophysics, and Cellular and Molecular Pharmacology

[4]California Institute for Quantitative Biomedical Research

[5]Kavli Institute for Fundamental Neuroscience

University of California, San Francisco, California 93858-2330 USA

[2]Molecular Biophysics and Integrated Bio-imaging Division

Lawrence Berkeley National Laboratory, Berkeley, CA 94720 USA

*Correspondence to: daniel.minor@ucsf.edu

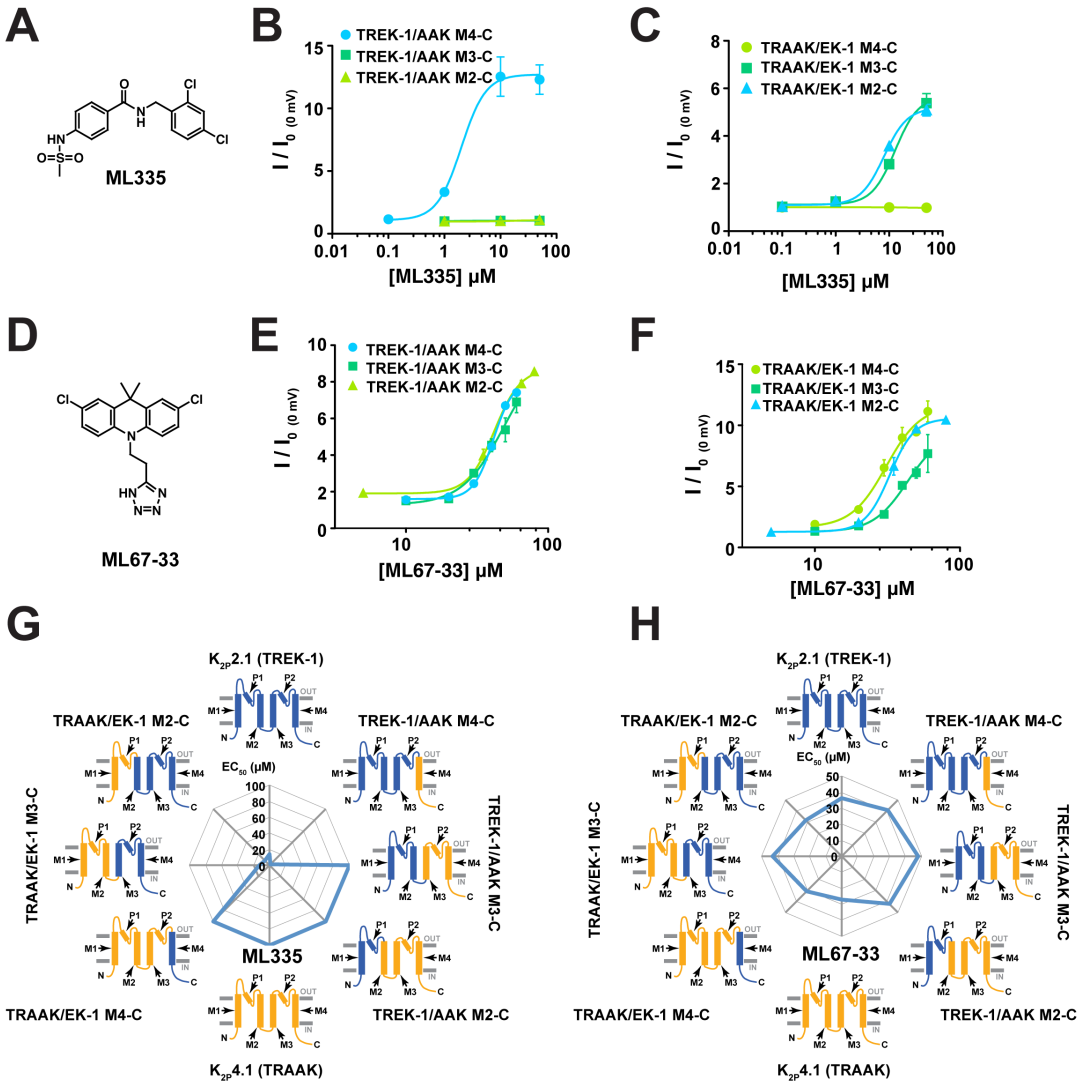

Figure S1 Responses of TREK-1/TRAAK chimeras to ML335 and ML67-33 activators. A, ML335 chemical structure. **B,** and **C,** ML335 dose-response curves for: TREK-1/AAK M4-C (light blue), TREK-1/AAK M3-C (green), and TREK-1/AAK M2-C (light green) (EC_{50} = 2.0 ± 0.6 µM, >100 µM, and >100 µM, respectively), and TRAAK/EK-1 M4-C (light green), TRAAK/EK-1 M3-C (green), and TRAAK/EK-1 M2-C (light blue) (EC_{50} = >100 µM, 13 ± 2 µM, and 8.0 ± 1.0 µM respectively). **D,** ML67-33 chemical structure. **E,** and **F,** ML67-33 dose-response curves for: TREK-1/AAK M4-C (light blue), TREK-1/AAK M3-C (green), and TREK-1/AAK M2-C (light green), (EC_{50} = 42 ± 3 µM, 49 ± 22 µM, and 42 ± 3 µM, respectively), and TRAAK/EK-1 M4-C (light green), TRAAK/EK-1 M3-C (green), TRAAK/EK-1 M2-C (light blue), (EC_{50} = 31 ± 3 µM, 44 ± 14 µM,, and 33 ± 1 µM, respectively). **G,** and **H**, Spider plot of EC_{50}s for the indicated chimeras. Cartoon schematics show channel portions from K_{2P}2.1(TREK-1) (blue) and K_{2P}4.1(TRAAK) (light orange). Error bars are s.e.m.

Figure S2

Pope *et al.*

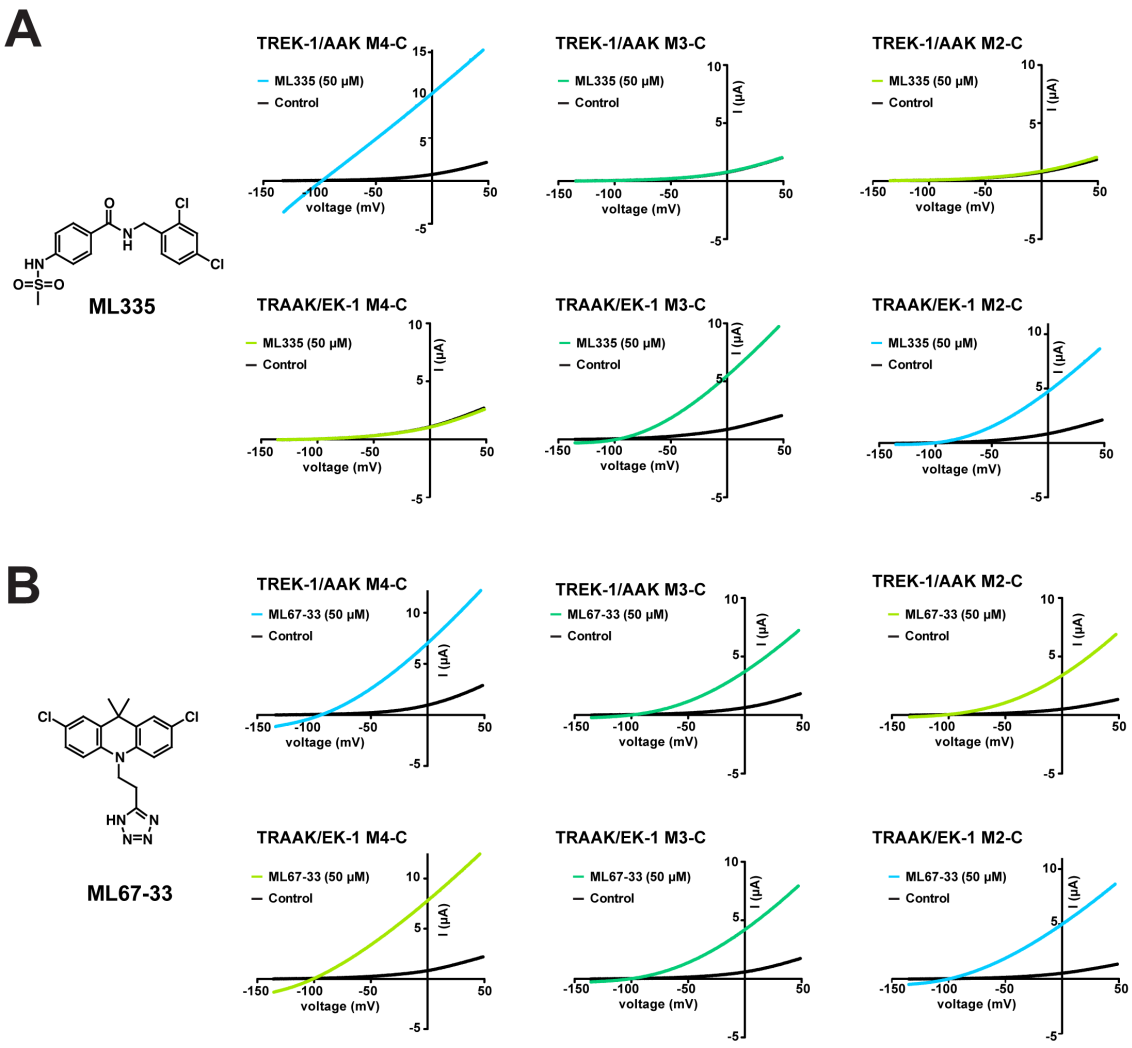

Figure S2 Exemplar responses of TREK-1/TRAAK chimeras to ML335 and ML67-33 activators. A, Chemical structure of ML335 and exemplars for responses of TREK-1/AAK M4-C (light blue), TREK-1/AAK M3-C (green), TREK-1/AAK M2-C (light green), TRAAK/EK-1 M4-C (light green), TRAAK/EK-1 M3-C (green), and TRAAK/EK-1 M2-C (light blue) to 50 µM ML335. **B,** Chemical structure of ML67-33 and exemplars for responses to 50 µM ML67-33. Colors are as in '**A**'.

Synthesis of BL-1249 analogs

General Procedures: Reactions were stirred magnetically unless otherwise indicated. Air and/or moisture sensitive reactions were carried out under an argon atmosphere in oven-dried glassware using anhydrous solvents from commercial suppliers. Air and/or moisture sensitive reagents were transferred via syringe or cannula and were introduced into reaction vessels through rubber septa. Reaction product solutions and chromatography fractions were concentrated by rotary evaporation at room temperature at 20 Torr then at 0.5 Torr unless otherwise indicated. Thin phase chromatography was performed on EMD precoated glass-backed silica gel 60 F-254 0.25 mm plate.

Materials: All chemical reagents and solvents used were purchased from Sigma-Aldrich or Fisher Scientific. Anhydrous dichloromethane and tetrahydrofuran (EMD Drisolv) were used without further purification

The following known compounds were prepared as detailed herein, based on the reported experimental procedures as described:

Preparation of **1**: WO2014/100818; (2014) (A1) English.
Preparation of **5**: *European Journal of Organic Chemistry*, 2017(1), 203-207; 2017
Preparation of **10**: *Med. Chem. Commun.*, 2012, 3, 373-378.
Preparation of **11**: *Med. Chem. Commun.*, 2012, 3, 373-378.
Preparation of **13**: *Journal of Medicinal Chemistry,* 2001, 44 (26) 4524-4534

Synthetic Procedures

2-[(5,6,7,8-tetrahydronaphthalen-1-yl)amino]benzonitrile (1): To an oven-dried, septum-capped, 40 mL vial was added 2-amino-5,6,7,8-tetrahydronaphthalene (260 mg , 1.0 mmol), 4,5-bis(diphenylphosphino)-9,9-dimethylxanthene (79 mg, 0.1 mmol, 0.1 equiv.) and cesium carbonate (589 mg, 1.8 mmol, 1.3 equiv.), along with a stirbar. 2-Bromobenzonitrile (250 mg, 1.4 mmol, 1.0 equiv.) was dissolved in dry 1,4-dioxane (8.000 ml, 93.5 mmol, 68.8 equiv.) that had been degassed with dry nitrogen. The resulting solution was transferred to the vial with the other reagents, sealed, and the reaction mixture bubbled with dry nitrogen for 1 minute (with a needle used as a nitrogen outlet, this measure serves to purge the sealed vessel with inert gas). The reaction mixture was then stirred under dry nitrogen for 3 hours at 90°C, at which time TLC (10% EA/hexane) showed a new spot (UV_{254}) with $R_f \sim 0.6$. The reaction mixture was filtered through celite and concentrated to afford a residue that was dissolved in CH_2Cl_2 and loaded on a 40 g Silicycle cartridge, eluting with a gradient of 0-10% ethyl acetate in hexane. The fractions containing product were collected and concentrated to afford the product (208 mg, 1.1 mmol). (79%) ^{1}H NMR (300 MHz, $CDCl_3$) δ ppm 7.50 (dd, *J*=7.72, 1.70 Hz, 1 H), 7.34 (ddd, *J*=8.67, 7.25, 1.60 Hz, 1 H), 7.09 - 7.22 (m, 2 H), 6.97 - 7.05 (m, 1 H), 6.75 - 6.90 (m, 2 H),) 6.11 (s, 1 H), 2.78 - 2.93 (m, 2 H) 2.58 - 2.74 (m, 2 H) 1.74 - 1.92 (m, 4 H); LCMS (ESI) *m/z* $[M+H]^+$249.2, 250.2

2-[(5,6,7,8-tetrahydronaphthalen-1-yl)amino]benzoic acid (BL-1249 acid) and **2-[(5,6,7,8-tetrahydronaphthalen-1-yl)amino]benzamide (BL-1249 amide).** Intermediate [(5,6,7,8-tetrahydronaphthalen-1-yl)amino]benzonitrile (compound **1**, 31 mg, 0.1 mmol, 1.0 equiv.) was placed in a 4 mL screw-cap vial with a stirbar. This was dissolved in dimethyl sulfoxide (200 µL) and potassium hydroxide (167 µL, 1.0 mmol, 8.2 equiv.) was added. Finally, water (633 µL) was added to bring the final volume up to ~1 mL. The reaction mixture was capped and stirred at 105°C for 18 hours. After cooling, 6M HCl (~0.2 mL) was added slowly to bring the pH to zero. The reaction mixture was diluted with water and extracted twice with ethyl acetate. The combined organic layers were washed twice with brine then dried with sodium sulfate, filtered

and concentrated to afford the crude product. This was dissolved in a small amount of dichloromethane, loaded on a 4g Silicycle silica cartridge pre-equilibrated with hexane, and eluted with the following gradient: 3 column volumes (CV) hexane, then 0-100% EtOAc/hexanes over 12 CV. The fractions containing acid and amide products were collected and concentrated to afford **BL-1249 acid** and **BL-1249 amide**.

2-[(5,6,7,8-tetrahydronaphthalen-1-yl)amino]benzoic acid (3 mg, 0.012 mmol, 10%), **(BL-1249 acid).** ^{1}H NMR (300 MHz, $CDCl_3$) δ ppm 8.04 (dd, *J*=8.10, 1.51 Hz, 1 H) 7.31 (ddd, *J*=8.67, 6.97, 1.70 Hz, 1 H) 7.08 - 7.22 (m, 2 H) 6.88 - 7.00 (m, 2 H) 6.71 (ddd, *J*=8.10, 7.06, 1.04 Hz, 1 H) 2.84 (br d, *J*=6.03 Hz, 2 H) 2.67 (br d, *J*=5.84 Hz, 2 H) 1.73 - 1.88 (m, 4 H); ^{13}C NMR (126 MHz, $CDCl_3$) δ ppm 173.28 (s, 1 C) 149.76 (s, 1 C) 139.04 (s, 1 C) 138.33 (s, 1 C) 135.17 (s, 1 C) 132.46 (s, 1 C) 132.36 (s, 1 C) 126.03 (s, 1 C) 125.70 (s, 1 C) 121.77 (s, 1 C) 116.36 (s, 1 C) 113.87 (s, 1 C) 109.62 (s, 1 C) 29.86 (s, 1 C) 24.89 (s, 1 C) 22.98 (s, 1 C) 22.74 (s, 1 C); LCMS, $[M+H]^+$ = 268.2; LCMS, ESI$^-$ $[M-H]^-$ = 266.9

2-[(5,6,7,8-tetrahydronaphthalen-1-yl)amino]benzamide (16 mg, 0.060 mmol, 49%) **(BL-1249 amide).** ^{1}H NMR (300 MHz, $CDCl_3$) δ ppm 9.37 (s, 1 H) 7.47 (dd, *J*=7.91, 1.51 Hz, 1 H) 7.06 - 7.30 (m, 4 H) 6.87 (d, *J*=7.16 Hz, 1 H) 6.71 (ddd, *J*=7.96, 7.02, 1.22 Hz, 1 H) 5.92 (br s, 2 H) 2.81 (t, *J*=5.84 Hz, 2 H) 2.69 (t, *J*=5.93 Hz, 2 H) 1.66 - 1.88 (m, 4 H); ^{13}C NMR (75 MHz, $CDCl_3$) δ ppm 172.00 (s, 1 C) 147.41 (s, 1 C) 139.27 (s, 1 C) 138.89 (s, 1 C) 133.00 (s, 1 C) 130.82 (s, 1 C) 128.26 (s, 1 C) 125.51 (s, 1 C) 124.68 (s, 1 C) 119.26 (s, 1 C) 116.76 (s, 1 C) 115.23 (s, 1 C) 115.03 (s, 1 C) 77.48 (s, 1 C) 77.06 (s, 1 C) 76.63 (s, 1 C) 29.99 (s, 1 C) 24.85 (s, 1 C) 23.07 (s, 1 C) 22.80 (s, 1 C); LCMS, $[M+H]^+$ = 250.2 (m-H_2O + 1)

N-phenyl-2-(1H-1,2,3,4-tetrazol-5-yl)aniline (BL-1249-Ph): A septum capped 40 mL vial was charged with 2-(phenylamino)benzonitrile (compound **2**, 35 mg, 0.2 mmol, 1.0 equiv.), sodium azide (38 mg, 0.6 mmol, 3.3 equiv.) and ammonium chloride (32 mg, 0.6 mmol, 3.6 equiv.). Dry DMF (1.5 mL) was added and the tube was flushed with dry nitrogen and sealed. The tube was then heated at 120°C overnight with stirring. The reaction mixture was cooled, diluted with water, and the pH of the solution determined to be ~5. The slurry was

extracted with ethyl acetate once, then twice with 20% MeOH in CH_2Cl_2, and the combined organic layer washed with brine, dried with sodium sulfate, filtered, and concentrated. The crude residue was loaded atop a 4 g column of silica gel and eluted with 0 to 10% methanol in CH_2Cl_2. The fractions containing product were collected and concentrated to afford the title compound (12.9 mg, 31%). ^{1}H NMR (300 MHz, METHANOL-*d*$_4$) d ppm 7.80 (dd, *J*=7.44, 0.85 Hz, 1 H) 7.27 - 7.42 (m, 4 H) 7.18 - 7.25 (m, 2 H) 7.00 - 7.08 (m, 1 H) 6.94 (ddd, *J*=8.01, 6.12, 2.07 Hz, 1 H); LCMS (ESI) *m/z* $[M+H]^+$238.2

2-bromo-N-phenylaniline (5). To a solution of commercially available *o*-bromoaniline (**4**, 4.32g, 2.84 mL, 25 mmol) in MeCN (30 mL), was added silylaryl triflate (**3**, 5.0g, 4.0 mL, 16.8 mmol) and 2 equivalents of CsF (7.6 g, 50 mmol). The reaction mixture was allowed to stir at room temperature and monitored by TLC. When judged complete, the reaction mixture was washed with brine (20 mL) and extracted with ether (3x30 mL). The combined ether fractions were dried over Na_2SO_4 and concentrated under reduced pressure. The crude residue was purified by silica gel column chromatography (Hex:EtOAc 10-40%) to afford the desired product as a colorless oil (3.83 g, 92%). ^{1}H NMR (300 MHz, CHLOROFORM-*d*) δ ppm 7.52 - 7.62 (m, 1 H) 7.32 - 7.42 (m, 2 H) 7.26 - 7.32 (m, 1 H) 7.15 - 7.25 (m, 2 H) 7.03 - 7.13 (m, 1 H) 6.73 - 6.84 (m, 1 H) 6.12 (br. s., 1 H); LCMS (ESI^+) m/z 249 ($M+H^+$).

Tert-butyl N-(2-bromophenyl)-N-phenylcarbamate (6): To a solution of 2-bromo-N-phenylaniline (**5**, 3.84 g, 15.4 mmol) in THF (20 mL), was added a solution of Boc_2O (5.05g, 23.1 mmol) in THF (5 mL) along with a catalytic amount of DMAP. The reaction mixture was stirred for 3 hours at 40°C until reaction was judged complete by LC/MS analysis. Excess DMAP was then added and the reaction mixture stirred for another 30 min, in an attempt to decompose the excess Boc_2O. Water (100 mL) was then added to mixture, which was extracted with EtOAc (3x30 mL). The combined organic layers were dried over anhydrous $MgSO_4$, filtered and evaporated under reduced pressure. The crude oil was purified using silica gel column chromatography (Hex:EtOAc/0-50%) to afford the desired product (4.38 g, 81.6% yield) as a colorless oil that solidified. ^{1}H NMR (300 MHz, DMSO-*d*$_6$) δ ppm 7.69 - 7.79 (m, 1 H) 7.42

(dd, *J*=4.14, 0.94 Hz, 2 H) 7.20 - 7.37 (m, 5 H) 7.09 - 7.20 (m, 1 H) 1.36 (s, 9 H); (ESI^+) m/z 349 ($M+H^+$).

1-phenylspiro[3,1-benzoxazine-4,1'-cyclohexane]-2-one (7): A flame-dried flask charged with *t*-butyl N-(2-bromophenyl)-N-phenylcarbamate (**6**, 1.68 g, 4.8 mmol, 1.0 equiv.) and dry THF (12 mL) under argon and cooled to -78°C. Tert-butyllithium (5.681 mL, 9.7 mmol, 2.0 equiv.) was added dropwise over 5 min. The reaction was stirred at -78°C for 5 min and treated dropwise with a solution of cyclohexanone (711 mg, 748 mL, 7.2 mmol, 1.5 equiv.) in 3 mL dry THF. The reaction mixture was stirred for 5 min and then quenched at -78°C with 30 mL water. The mixture was warmed to room temperature and partitioned between ethyl acetate and water. The layers were separated and the aqueous phase extracted twice more with ethyl acetate. The combined organic phases were washed with brine, dried over $MgSO_4$, filtered and concentrated. The crude residue was purified on a 40g Silicycle column eluting with 0 to 60% EtOAc/hexane to afford 1-phenyl-1,2-dihydrospiro[3,1-benzoxazine-4,1'-cyclohexane]-2-one **(7)** (1.072 g, 3.7 mmol, 76%)**.** ^1H NMR (300 MHz, DMSO-d_6) δ ppm 7.45 - 7.63 (m, 3 H) 7.33 - 7.45 (m, 3 H) 7.05 - 7.24 (m, 2 H) 6.20 (d, *J*=7.72 Hz, 1 H) 2.09 - 2.22 (m, 2 H) 1.86 - 2.02 (m, 2 H) 1.71 - 1.78 (m, 2 H) 1.59 - 1.85 (m, 4 H) 1.27 - 1.46 (m, 1 H); LCMS (ESI^+) m/z 294.0 ($M+H^+$)

1-[2-(phenylamino)phenyl]cyclohexan-1-ol (8): To a solution of 1-phenylspiro[3,1-benzoxazine-4,1'-cyclohexane]-2-one (**7**, 1.50 g, 5.11 mmol) in EtOH (5.0 mL) was added 3 equivalents of 5M NaOH (3.07 mL). The reaction mixture was heated to reflux for 8 hours, cooled, and stirred at room temperature overnight. The reaction mixture was then poured into ice/water and 0.5M HCl was added until the solution tested at pH ~7. This solution was then extracted with CH_2Cl_2 (2x20mL), dried over anhydrous $MgSO_4$, filtered and concentrated. The crude product was purified on a 25g Silicycle cartridge eluting with 0 to 40% EtOAc/hexanes over 12 column volumes to afford the title compound (1.03g, 3.86 mmol, 75%). ^1H NMR (300 MHz, DMSO-d_6) δ ppm 8.57 (s, 1 H) 7.07 - 7.37 (m, 4 H) 6.98 (d, *J*=8.48 Hz, 2 H) 6.72 - 6.93

(m, 2 H) 5.54 (s, 1 H) 1.90 - 2.11 (m, 3 H) 1.56 - 1.84 (m, 4 H) 1.48 (d, *J*=12.62 Hz, 2 H) 1.17 (t, *J*=7.16 Hz, 2 H) LC/MS (ESI^+) m/z 268.0 ($M+H^+$)

10H-spiro[acridine-9,1'-cyclohexane] (9): A mixture of 1-[2-(phenylamino)phenyl]cyclohexan-1-ol (**8**, 749 mg, 2.80 mmol) in 85% phosphoric acid (12 mL) was stirred at room temperature for 4 hours, at which time the reaction was judged complete by TLC. The reaction mixture was poured into water and the product was extracted with EtOAc (2x20mL). The combined organic phases were then dried over anhydrous $MgSO_4$, filtered and evaporated under reduced pressure. The crude product was purified using silica gel column chromatography (HexEtOAc/ 0-40%) over 12 column volume on a 40g Silicycle cartridge. As this insoluble intermediate precipitated in the lines of the Biotage flash chromatography system, it is strongly advised that manual silica gel flash chromatography be used to purify this intermediate. The fractions containing product were collected and concentrated to afford the title compound (534 mg, 77% yield) as an oil that solidified upon standing. ^1H NMR (400 MHz, DMSO-d_6) δ ppm 8.92 (s, 1 H) 7.40 - 7.46 (m, 2 H) 7.04 - 7.11 (m, 2 H) 6.94 (dd, *J*=7.91, 1.34 Hz, 2 H) 6.89 (td, *J*=7.49, 1.34 Hz, 2 H) 1.82 - 1.93 (m, 4 H) 1.52 - 1.61 (m, 4 H) 1.48 (d, *J*=4.63 Hz, 2 H); ^{13}C NMR (100 MHz, DMSO-d_6) δ ppm 140.99 (s, 1 C) 128.27 (s, 1 C) 125.90 (s, 1 C) 124.79 (s, 1 C) 119.80 (s, 1 C) 113.97 (s, 1 C) 38.84 (s, 1 C) 32.70 (s, 1 C) 25.83 (s, 1 C) 22.77 (s, 1 C) LCMS (ESI^+) m/z 250.1 ($M+H^+$)

10H-spiro[acridine-9,1'-cyclohexane]-5-carbaldehyde (10): 10H-spiro[acridine-9,1'-cyclohexane] (**9**, 500 mg, 2.01 mmol) in diethyl ether (10 ml) was cooled to -78 ^{o} C and treated with n-butyl lithium (2.5 M, 2.41 mL, 6.02 mmol) and then allowed to warm to room temperature and stirred for four days. DMF (0.232 mL, 3.01 mmol) was added and the reaction mixture was stirred for an additional 24 hours, after which the reaction mixture was quenched with excess 0.5 M aqueous HCl. The solution was extracted with ether and the combined organics were washed with brine, dried over sodium sulfate, filtered, and concentrated. The crude product was purified on a 40 g Silicycle cartridge eluting with 0-10 % EtOAc/hexanes. To further purify the product and separate it from residual starting material, the product obtained

from chromatography was triturated with hexane, with the product predominantly in the hexane phase. TLC and ^{1}H NMR showed that the product was still impure, and it was therefore carried onto the next step without further purification. For the crude product: ^{1}H NMR (300 MHz, CHLOROFORM-*d*) δ ppm 10.58 (br. s., 1 H), 10.01 (s, 1 H) 7.73 - 7.82 (m, 1 H), 7.54 - 7.62 (m, 1 H), 7.50 (dd, *J*=7.54, 1.32 Hz, 1 H) 6.99 -7.27 (m, 4 H), 6.87 (dd, *J*=7.72, 1.13 Hz, 1 H), 6.33 (br. s., 1 H) , 1.98 - 2.17 (m, 4 H) 1.52 - 1.83 (m, 6 H)

10H-spiro[acridine-9,1'-cyclohexane]-4-carboxylic acid (11): The crude 10H-spiro[acridine-9,1'-cyclohexane]-5-carbaldehyde (**10**, 453 mg, 1.63 mmol) from the previous step was dissolved in t-BuOH:water (4:1, 90 mL) and treated with NaH_2PO_4 hydrate (1.80 g, 13.1 mmol), 2-methyl-2-butene (1.73 mL, 6.54 mmol) and $NaClO_2$ (448 mg, 6.54 mmol), and then stirred overnight. The organics were then removed by rotary evaporation and the remaining aqueous mixture was partitioned between ether and 2 M aq. NaOH. The ether layer was separated and the aqueous layer was acidified with aqueous HCl to pH ~2 forming a milky solution that was extracted with ethyl acetate. The combined organic phases were washed with brine, dried over sodium sulfate, filtered, and concentrated. The crude product was purified on a 12g Silicycle column eluting with 0-10% MeOH/CH_2Cl_2 to afford the product (77.8 mg, 21.5 % over 2 steps). ^{1}H NMR (300 MHz, CHLOROFORM-*d*) δ ppm 1.47 - 1.81 (m, 6 H) 1.96 - 2.16 (m, 4 H) 6.92 - 7.11 (m, 3 H) 7.15 - 7.25 (m, 1 H) 7.47 - 7.59 (m, 1H) 7.71 - 7.80 (m, 1 H) 8.01 (dd, *J*=7.91, 1.32 Hz, 1 H) 10.10 (s, 1 H) ^{13}C NMR (CHLOROFORM-*d* 75 MHz,) δ ppm 23.19 (s, 1 C) 26.33 (s, 1 C) 33.27 (s, 1 C) 39.65 (s, 1 C) 109.87 (s, 1 C) 115.55 (s, 1 C) 119.04 (s, 1 C) 121.70 (s, 1 C) 124.90 (s, 1 C) 126.39 (s, 1 C) 129.33 (s, 1 C) 130.84 (s, 1 C) 131.78 (s, 1 C) 138.91 (s, 1 C) 144.58 (s, 1 C) 174.07 (s, 1 C)

10H-spiro[acridine-9,1'-cyclohexane]-5-carboxamide (12): The intermediate 10H-spiro[acridine-9,1'-cyclohexane]-4-carboxylic acid (**11**, 58.7 mg, 0.200 mmol) was dissolved in THF (3 mL) and the mixture treated with 1-(3-dimethylaminopropyl)-3-ethylcarbodiimide hydrochloride (115 mg, 0.600 mmol), 1-hydroxybenzotriazole hydrate (92 mg, 0.600 mmol), ammonium chloride (49.5 mg, 1.00 mmol), and trimethylamine (0.139 mL, 5 mmol). The

reaction mixture was stirred for 18 hours at room temperature. The solvent was evaporated and the residue dissolved in ethyl acetate and washed with half saturated aqueous $NaHCO_3$. The organic phase was washed with brine, dried over sodium sulfate, filtered, and concentrated. The crude residue was purified on a 12 g Silicycle cartridge eluting with 0-100% EtOAc/hexanes to afford the product (41.2 mg, 0.141 mmol, 70%). ^{1}H NMR (300 MHz, CHLOROFORM-*d*) δ ppm 10.50 (s, 1 H) 7.66 (d, *J*=7.72 Hz, 1 H) 7.48 - 7.55 (m, 1 H) 7.36 (dd, *J*=7.91, 0.94 Hz, 1 H) 7.12 - 7.21 (m, 1 H) 7.02 (td, *J*=7.54, 1.32 Hz, 1 H) 6.88 - 6.99 (m, 2 H) 6.07 (br. s., 2 H) 1.95 - 2.06 (m, 3 H) 1.47 - 1.76 (m, 5 H) ^{13}C NMR (75 MHz, CHLOROFORM-*d*) δ ppm 172.00 (s, 1 C) 143.19 (s, 1 C) 139.44 (s, 1 C) 131.28 (s, 1 C) 129.53 (s, 1 C) 128.92 (s, 1 C) 126.23 (s, 1 C) 124.84 (s, 1 C) 124.69 (s, 1 C) 121.11 (s, 1 C) 118.70 (s, 1 C) 115.34 (s, 1 C) 113.36 (s, 1 C), (s, 1 C) 39.63 (s, 1 C) 33.00 (s, 1 C) 26.31 (s, 1 C) 23.15 (s, 1 C); LCMS, ESI$^+$ $[M+H]^+$: 292.6

10H-spiro[acridine-9,1'-cyclohexane]-5-carbonitrile (13) To dry DMF (~1 mL) at 0 ^{o}C, oxalyl chloride (0.016 mL, 0.19 mmol) was slowly added via syringe. The mixture was stirred for five minutes and then dry pyridine (0.034 mL, 0.38 mmol) was added, followed by a solution of 10H-spiro[acridine-9,1'-cyclohexane]-5-carboxamide (**12**, 27.6 mg, 0.094 mmol) dissolved in dry DMF (0.75 ml). The reaction was allowed to proceed in the ice bath until the reaction was complete as judged by TLC. The reaction mixture was diluted with ethyl acetate and washed with saturated aqueous lithium chloride. The lithium chloride solution was extracted again with ethyl acetate. The combined organics were washed with brine, dried over sodium sulfate, filtered and concentrated. The crude product was purified on a 12 g Silicycle cartridge eluting with 0-20% EtOAc/hexanes to afford the title compound (18.4 mg, 0.067 mmol, 71%). ^{1}H NMR (300 MHz, CHLOROFORM-*d*) δ ppm 7.69 - 7.76 (m, 1 H) 7.51 - 7.58 (m, 1 H) 7.40 (dd, *J*=7.72, 1.13 Hz, 1 H) 7.21 (td, *J*=7.54, 1.32 Hz, 1 H) 7.09 (td, *J*=7.54, 1.32 Hz, 1 H) 6.93 - 7.04 (m, 3 H) 1.91 - 2.10 (m, 4 H) 1.49 - 1.76 (m, 6 H) ^{13}C NMR (75 MHz, CHLOROFORM-*d*) δ ppm 143.12 (s, 1 C) 138.40 (s, 1 C) 130.62 (s, 1 C) 130.24 (s, 1 C) 129.29 (s, 1 C) 129.11 (s, 1 C) 126.65 (s, 1 C) 125.25 (s, 1 C) 122.28 (s, 1 C) 120.42 (s, 1 C) 117.41 (s, 1 C) 114.94 (s, 1 C) 96.17 (s, 1 C), 39.74 (s, 1 C) 33.18 (s, 1 C) 26.04 (s, 1 C) 23.03 (s, 1 C), LCMS, ESI$^+$ $[M+H]^+$: 275.5, 276.5

5-(1H-1,2,3,4-tetrazol-5-yl)-10H-spiro[acridine-9,1'-cyclohexane (BL-1249 tricycle) A sealed septum-capped vessel was charged with 10H-spiro[acridine-9,1'-cyclohexane]-5-carbonitrile (**13**, 16.5 mg, 0.060 mmol), sodium azide (13 mg, 0.2 mmol, 3.3 equiv.) and ammonium chloride (11 mg, 0.2 mmol, 3.6 equiv.). Dry DMF (1.5 mL) was added and the tube was flushed with dry nitrogen and sealed. The tube was then heated at 120°C 18 hrs with stirring in an aluminum heating block. The reaction mixture was cooled to room temperature, diluted with water, and the pH was adjusted to ~5 by addition of a few drops 1N HCl. The slurry was extracted with ethyl acetate once, then twice with 20% MeOH in CH_2Cl_2, and the organic layer washed with brine, dried with sodium sulfate, filtered, and concentrated. The residue was purified on a 12g Silicycle cartridge eluting with 0-10% MeOH/CH_2Cl_2 over 12 CV. After collecting and concentrating the relevant column fractions, the product contained residual DMF. The product was therefore dissolved in CH_2Cl_2, extracted with brine, dried with sodium sulfate, filtered and concentrated to afford the product (10 mg, 0.032 mmol, 53 %), ^{1}H NMR (400 MHz, METHANOL-*d*4) δ ppm 7.70 - 7.75 (m, 1 H) 7.69 (dd, J=7.79, 1.22 Hz, 1 H) 7.52 (dd, J=7.67, 0.85 Hz, 1 H) 7.06 - 7.17 (m, 2 H) 6.97 - 7.03 (m, 2 H) 1.96 - 2.09 (m, 4 H) 1.48 - 1.71 (m, 6 H); ^{13}C NMR (100 MHz, METHANOL-*d*4) δ ppm 24.44 (s, 1 C) 27.59 (s, 1 C) 34.31 (s, 1 C) 41.20 (s, 1 C) 108.12 (s, 1 C) 116.31 (s, 1 C) 121.22 (s, 1 C) 122.62 (s, 1 C) 126.19 (s, 1 C) 126.24 (s, 1 C) 127.60 (s, 1 C) 129.58 (s, 1 C) 130.40 (s, 1 C) 132.73 (s, 1 C) 141.08 (s, 1 C) 141.47 (s, 1 C) 157.17 (s, 1 C)

Scheme 1: BL-1249-acid, BL-1249-amide, BL-1249-Ph

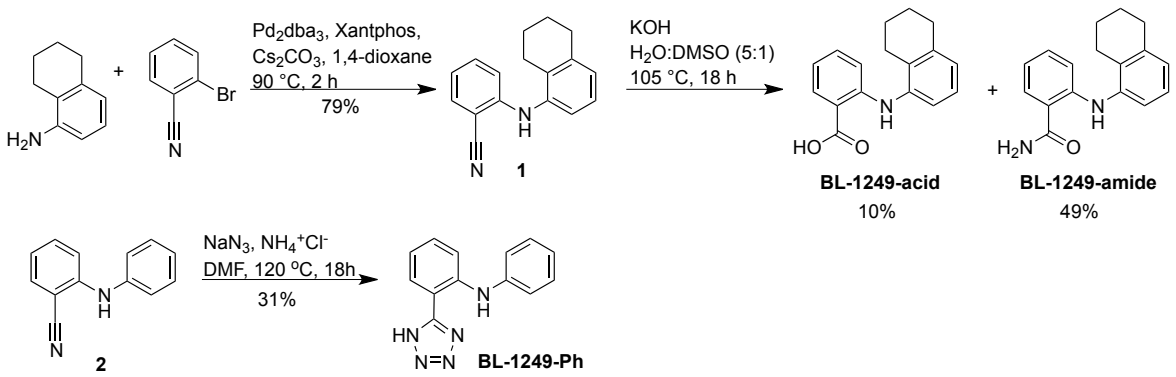

Scheme 2: BL-1249-tricycle